62p

Copy 40

NASA TM X-785

NASA TM X-785

X63-12013

Code 2

TECHNICAL MEMORANDUM

X-785

AN EXPERIMENTAL INVESTIGATION OF THE CONVECTIVE HEAT TRANSFER TO A BLUNT LIFTING BODY WITH CONTROLS

By H. Lee Seegmiller and John O. Reller, Jr.

Ames Research Center
Moffett Field, Calif.

NATIONAL AERONAUTICS AND SPACE ADMINISTRATION
WASHINGTON
April 1963

NATIONAL AERONAUTICS AND SPACE ADMINISTRATION

TECHNICAL MEMORANDUM X-785

AN EXPERIMENTAL INVESTIGATION OF THE CONVECTIVE HEAT TRANSFER TO A BLUNT LIFTING BODY WITH CONTROLS*

By H. Lee Seegmiller and John O. Reller, Jr.

SUMMARY

The convective heating of a blunt lifting body with controls was measured at a Mach number of 5 and a stream stagnation enthalpy of 160 Btu per pound in a steady flow wind tunnel and at a Mach number of 10 and stream stagnation enthalpy of 4000 Btu per pound in a combustion driven shock tunnel. The body was tested at angles of attack from $+6.5^{\circ}$ to -14° and consisted of the lower half of a blunt 30° semiapex angle cone with a flat upper section inclined 6.6° to the cone axis. This shape is often termed the M-1 configuration. The free-stream Reynolds numbers based on maximum body diameter were 0.72×10^{6} in the wind tunnel and 0.012×10^{6} for the shock-tunnel test. The heating distributions obtained at the two test conditions were similar over the nose and conical surface of the body; however, the shock-tunnel data were found to indicate somewhat lower heating on the forward areas of the flat upper surface. At both test conditions, the data for the body at angles of attack of 0° and -14° were found to agree well with theoretical estimates for laminar flow. Base heating was measured in the wind tunnel and found to vary from 1 percent to about 8 percent of the body stagnation value.

Trailing flap-type controls were tested and under some conditions evidenced heating in excess of that at the body stagnation point. For controls mounted aft of the flat upper surface near the outer edge of the body there were large lateral and longitudinal variations in heating at large deflection angles. Some evidence of intense heating of the body surface adjacent to the upper controls at large deflection angles was also noted. Heating of the leading edge of small triangular elevonlike controls was in reasonable agreement with theoretical estimates for a swept cylinder, and varied from about 0.6 to 0.8 of the body stagnation value.

INTRODUCTION

Numerous studies have shown that the use of relatively small amounts of lift can have significant effects on the motion and heating of vehicles entering planetary atmospheres (e.g., refs. 1-4). Based on these studies, entry vehicles

with lift-drag ratios as low as one-half can be attractive for many applications, particularly for manned missions. Among the suitable shapes with low lift-drag ratio are the so-called lifting bodies. A lifting body having a maximum lift-drag ratio near one-half and consisting of essentially one-half of a blunt 30° half-angle cone was introduced by Eggers and Wong in reference 5. This shape is often referred to as the M-1.

Since its introduction the M-1 configuration has been the subject of numerous investigations (see refs. 6 to 14). The majority have been focused on its force and stability characteristics; however, a study of the convective heating was begun in reference 10. The present paper contains the results of additional studies of the heat-transfer characteristics of the configuration. The convective heating is examined at two widely different enthalpy levels and the measured results are compared with theoretical estimates. Considerable attention is directed toward the heating of several aerodynamic controls, and exploratory measurements of base heating at low enthalpy will also be presented.

SYMBOLS

C	specific heat of model shell material
c_p	specific heat of air at constant pressure
C_p	pressure coefficient
D	body diameter
G	model semigirth coordinate
h	heat-transfer coefficient
H	enthalpy
L	control-flap length coordinate
M	Mach number
$\dot{q}$	heat-transfer rate
r_o	body nose radius
R	model base coordinate
Re	Reynolds number
S'	body surface distance from intersection of cone axis and hemispherical nose
t	time

	temperature
W	control-flap width coordinate
X	model longitudinal coordinate
Y	model lateral coordinate
Z	vertical coordinate from model
α	body angle of attack measured relative to upper surface
δ	control deflection angle
ρ	density of model shell material
φ	body coordinate in roll plane
τ	model local shell thickness

Subscripts

AW	adiabatic wall
D	based on maximum body diameter
EW	equilibrium wall
o	reference stagnation-point heating at $\alpha = 0^{\circ}$
t	total distance
T	stagnation conditions
W	wall conditions
∞	free-stream conditions
2	conditions behind normal shock wave

EXPERIMENT

Test Facilities

Tests were conducted in the Ames 10- by 14-inch supersonic wind tunnel and the Ames 1-foot hypervelocity shock tunnel. A description of the 10- by 14-inch tunnel, which is a continuous flow type, may be found in reference 15. Tunnel conditions for the present tests were $M_\infty = 5.0$, $P_T = 86$ psia, $T_T = 200^\circ$ F, and $Re_D = 0.72 \times 10^6$.

The Ames 1-foot hypervelocity shock tunnel (see ref. 16) is a combustion-heated, shock-driven facility in which hydrogen and oxygen are ignited in a mixture with helium to produce a large volume of high-temperature, high-pressure gas. This gas is used to shock compress the test fluid (air), which then expands through a nozzle to the test chamber. Nominal test conditions during the data taking period were: $M_\infty = 10$, stream total enthalpy 4000 Btu/lb, $Re_D = 0.012 \times 10^6$, and stream velocity 13,800 ft/sec. Analysis of the stream calibration measurements has indicated the possibility of small departures from chemical equilibrium in the nozzle flow. It is believed, however, that measured heating distributions are unaffected by these small departures from chemical equilibrium.

Models

The models and nose coordinates are shown in figure 1. The body consists of the lower half of a blunted 30° semiapex angle cone with a flat top section inclined 6.6° to the cone axis. Body angle of attack, α, is measured relative to this flat top surface. The modified nose contour, described by Sarabia in reference 6, was used for the present tests. The four trailing flap-type controls shown in figure 1(a) are referred to as control set I and have an aspect ratio of 0.6. Control set II is shown in figure 1(b) and consists of two aspect-ratio-1.0 pitch controls and two aspect-ratio-0.6 yaw controls. Small elevonlike controls were tested separately and are shown in figure 1(c). The twin supports which were used for base heating and pressure measurements are sketched in figure 1(d). These supports were attached to the body at the normal location of the control-set-I upper flaps.

The models used for these tests were drawn from a flat type-321 stainless-steel sheet 0.015 inch thick. The wall thickness of the completed models was considerably less than this, however, and varied from about 0.006 inch at the nose to about 0.010 inch at the base.

The finished shells were fastened to a support ring with either soft solder or spot welds. Models employing each type of construction were tested in the 10- by 14-inch wind tunnel with comparable results. The flat base of the model was cut from 0.010 inch thick type-321 stainless-steel sheet and was insulated from the body. The controls were also insulated from the base with

[redacted]

ion spacers. The flap-type controls were formed of a flat type-321 stainless-steel sheet 0.015 inch thick. The elevons were also formed from a type-321 stainless-steel sheet which was rolled to 0.007-inch thickness before being formed.

Instrumentation

Model skin temperature was measured with 0.005-inch-diameter copper-constantan and iron-constantan thermocouples. Three hot-junction configurations were employed: (a) both wires silver soldered into individual drilled holes in the skin, (b) wires butt welded together and silver soldered to the inside skin surface, and (c) both wires individually spot welded to the inside skin surface. The test results showed no effect of the variations in thermocouple materials or installation techniques. For tests in the 10- by 14-inch supersonic wind tunnel, the cold junctions were placed in a dielectric silicone-oil bath which was maintained at 32° F. Because of the short times involved in the shock-tunnel tests, a room-temperature reference was used.

Thermocouple outputs were recorded as a function of time with a recording oscillograph during tests in both facilities. Outputs from several thermocouples were also monitored with oscilloscopes during the tests in the shock tunnel. Amplifiers were used for the shock-tunnel tests to obtain the required sensitivity from the fast-response galvanometer elements that were used.

Over-all instrumentation response was important for the tests in the shock tunnel and it was checked by impressing on each channel a sawtooth signal of proper frequency and strength to simulate a thermocouple output. The oscillograph traces were found to be linear within the accuracy of measurement and the time delay associated with the change in slope was found to be approximately 5 milliseconds. Since the transient thermal response time of the model skin varied from 3 to 15 milliseconds, the data were evaluated at times greater than 15 milliseconds after the start of flow. System response was not checked for the tests in the 10- by 14-inch wind tunnel since amplifiers were not used and the required time response of the galvanometers was well within rated performance.

Test Procedure

Data were obtained in both test facilities by the use of the thin-shell transient-temperature technique. With this technique, the model is exposed to a sudden change in environment and the time rate of change of the model shell temperature is determined. In the shock tunnel the facility itself provided the sudden change in conditions. In the wind tunnel a slightly different procedure was used and two types of data were obtained, heat-storage rate and equilibrium surface temperature. The equilibrium surface temperatures were measured first by recording model temperatures at the desired test condition until equilibrium was obtained. Heat-storage rates were then obtained with the following

[redacted]

technique. Liquid nitrogen was injected in the wind-tunnel settling chamber just upstream of the supersonic nozzle. After sufficient cooling was achieved (the temperature depression varied from 100° to 250° F) the flow of coolant was stopped. Thermocouple output as a function of time was then recorded as the tunnel stream warmed the model.

High-speed color motion pictures and short-time-duration still pictures were taken during the shock-tunnel tests and shadowgraphs were taken during tests in the wind tunnel.

Data Reduction and Accuracy

Heat balance.- A heat balance for the model skin may be written as:

$$\dot{q}_{stored} = \dot{q}_{convection\ net} + \dot{q}_{radiation\ net} + \dot{q}_{conduction\ net}$$

The quantity $\dot{q}_{radiation\ net}$ was estimated and found to be negligible for both test conditions. Convective heating or cooling of the interior surface was also found to be negligible because of the very low density of the air within the model. Because of the difficulties involved in the instrumentation of small models to define adequately the local skin temperature gradients, the following procedure was devised to estimate the effects of skin conduction on the heat-storage rates measured in the wind tunnel.

The measured heat-storage rates were plotted as a function of skin temperature beginning with coolant shut off and continuing until the temperature rise rates diminished to a low value. If the net conduction is negligible and if the heat-transfer coefficient and the adiabatic wall temperature are constant, a linear relationship should be obtained between heating rate and model wall temperature. The heat balance equation then becomes: $\dot{q}_{convection} = \dot{q}_{stored}$. The intercept for zero heating rate should occur at the adiabatic wall temperature and the slope of the curve is equal in magnitude to the heat-transfer coefficient. This result follows from the basic definition of heat-transfer coefficient in the equation:

$$h = \frac{\dot{q}_{convection}}{T_{AW} - T_W}$$

Curves of this type which are representative of the upper and lower levels of heating experienced by the wind-tunnel model are shown in figures 2 and 3. Both heat-storage rates and heat-transfer coefficients are plotted as a function of wall temperature for locations at the model nose and on the flat upper surface. It is seen that during the heating cycle a period of linear variation of heat-storage rate with wall temperature (and hence constant heat-transfer coefficient) does occur. Only data obtained in such periods were considered free of conduction effects and are presented. Since the same type of model was used in the shock tunnel where the convective heating rates are approximately two

ders of magnitude greater and the time scale is considerably compressed, it was assumed that the ratio of the net conducted heat to the convected heat was also negligible during the shock-tunnel tests.

The heat-storage rate was calculated from the relation:

$$\dot{q}_{stored} = \rho C \tau \frac{dT}{dt}$$

where ρ and C are the density and specific heat of the model skin, τ is the local skin thickness, and dT/dt is the temperature rise rate which was determined from the oscillograph record. The specific heat used was taken from reference 17.

Data presentation.- The data from the shock tunnel will be presented in the form of the dimensionless ratio of local heating to the body stagnation-point heating which occurred at 0° angle of attack. The data from the wind tunnel will be presented as the ratio of heat-transfer coefficients. A comparison of these two forms of heating parameters may be made in the following manner.

From the usual definition of heat-transfer coefficient,

$$h = \frac{\dot{q}}{T_{AW} - T_W}$$

a heat-transfer coefficient more applicable to higher enthalpies may be defined as:

$$h = \frac{\dot{q}}{\frac{H_{AW} - H_W}{c_p}}$$

where h is based on the enthalpy potential and c_p is evaluated at some reference condition. The ratio of local heat-transfer coefficient to the stagnation-point heat-transfer coefficient is then:

$$\frac{h}{h_o} = \frac{\dot{q}}{\dot{q}_o}\left(\frac{H_T - H_W}{H_{AW} - H_W}\right)$$

Now, since the ratio H_W/H_T for the shock-tunnel tests was approximately 0.04 and for $H_{AW} \approx H_T$ it is seen that the relation may be written with small error as:

$$\frac{h}{h_o} = \frac{\dot{q}}{\dot{q}_o}\left(\frac{H_T}{H_{AW}}\right)$$

Further, on the windward areas of this blunt body the ratio H_T/H_{AW} for the shock-tunnel tests varies from about 1.0 on the nose and conical surface to about 1.10 on the flat top. Therefore, in lieu of an accurate means to evaluate local recovery enthalpies the shock-tunnel data in the form $\dot{q}/\dot{q}_o$ will be presented with the wind-tunnel data in the form h/h_o. The accuracy of this comparison is believed to be sufficient for the comparative purposes of this report, that is, approximately 10 percent. Notice that, in general, the ratio of heating rates will be lower than the ratio of heat-transfer coefficients.

The wind-tunnel data in the form of heat-transfer coefficients were computed from the relation:

$$h = \frac{\dot{q}_{stored}}{T_{EW} - T_W}$$

where T_{EW} is the measured local equilibrium wall temperature during "hot soak" prior to cooling and T_W is the local instantaneous wall temperature during the heating cycle. Measured equilibrium wall temperatures are compared with adiabatic wall temperatures and the results for the upper and lower surface meridians are presented in table I. The measured pressures reported in reference 6 were used with the theory of reference 18 in this calculation of adiabatic wall temperatures for the case of laminar flow at $\alpha = 0^o$. The comparison, in general, shows a relatively small effect of wall conduction at equilibrium on the results when it is recalled that the difference between equilibrium wall temperature and local wall temperature is the factor that enters the expression for heat-transfer coefficient. The largest conduction effects are found to occur on the flat upper surface. Because of the low heat-transfer coefficients prevalent in this area at small angle of attack, and the effect of the nonisothermal wall, to be discussed later, the top surface temperatures, as seen in figure 3, were higher than those of other areas of the body during the period of data evaluation. It is seen that temperatures as high as 80° F or 90° F are required to meet the criteria established for data reduction. The 9° F difference between the measured equilibrium wall temperature and the calculated adiabatic wall temperature could result in an uncertainty of approximately 14 percent in the heat-transfer coefficient. The dashed line in figure 3(a) is shown for comparison and represents the relation necessary to establish zero heat input at the calculated adiabatic wall temperature. Because the example just described necessarily represents a rather extreme condition occurring on a limited portion of the body at small angles of attack, the measured equilibrium wall temperatures were used throughout in the reduction of data.

Accuracy.- The accuracy of the various measurements has been estimated and the results, in general, are believed to be accurate within ±15 percent. A single exception is the data taken on the top surface of the wind-tunnel model at low angle of attack. These data are believed to be somewhat less accurate as a result of the uncertainty in equilibrium wall temperature just described and the effect of the nonisothermal wall which will be discussed later.

RESULTS AND DISCUSSION

Body Heating

Longitudinal heating distribution.- Before the heating distributions are discussed, it is of interest to examine the body pressure distribution shown in figure 4. The test data were taken from reference 6 and the dashed line represents modified Newtonian impact theory. The abscissa is the ratio of local surface distance to the principal nose radius. Note that the longitudinal distributions of body pressures are reasonably well represented by the theory with the principal differences occurring on the aft portion of the lower meridian at $\alpha = 0^{\circ}$ and on the upper meridian at both angles.

The present results will be shown in the form of the ratio of local heating to that which occurred at the stagnation point when the angle of attack was zero. Results for the stagnation point were presented with the initial part of this investigation which was reported in reference 10. The reference stagnation-point heat-transfer coefficient, h_o, used to normalize the wind-tunnel results is an average of measured data obtained from several runs and is 0.0264 Btu/ft^2 sec $^{\circ}$F. For comparison, the value 0.0269 Btu/ft^2 sec $^{\circ}$F was obtained with the theory of reference 19. The present shock-tunnel data were normalized with respect to the measured stagnation-point heating rate of each individual test which varied from about 340 to 370 Btu/ft^2 sec. The value 360 Btu/ft^2 sec was obtained from an estimate using the theory of reference 19.

Results for the measurement of heat transfer to the upper and lower body meridians are shown in figures 5 and 6. Wind-tunnel and shock-tunnel data are shown together in figure 5 and separately with angle of attack as a parameter in figure 6. In the theoretical calculations, the pressure coefficients presented by Sarabia in reference 6 were used for both test conditions. The data are compared with the laminar-flow theory of Lees (see ref. 20) at the nose and on the lower meridian of the cone. The laminar-flow theories of Van Driest and of Romig and Dore, given in references 21 and 22, respectively, were used to estimate the heating distribution of the flat upper surface. The curve labeled three-dimensional flow was obtained by increasing the two-dimensional result by $\sqrt{3}$. Heating of the forward portion of the flat upper surface, which begins at $S'/r_o = 0.8$, is seen in figure 5(a) to decrease from a level consistent with the prediction for three-dimensional flow to a value more characteristic of a two-dimensional flow.

It is noted that substantial differences in the two heating distributions (wind tunnel and shock tunnel) occurred in the upper surface region. Two effects to be considered in this comparison are the influence of Mach number on the body pressures and the influence of the nonisothermal wall present in the wind-tunnel tests. The higher Mach number in the stream of the shock tunnel affects the conversion to pressure ratios of the pressure coefficients presented in figure 4. Specifically, it was found that for a given pressure coefficient the upper surface pressure was considerably reduced relative to the stagnation pressure for the higher Mach number. In part, this difference accounts for the lower relative

level of heating on the upper surface in the shock-tunnel tests. In this connection, it should be noted that the pressures obtained as just described were used with the theory of Romig and Dore (ref. 22) to obtain the estimates shown in figure 5(a), and reasonable agreement with experimental results was obtained. The second factor to consider involves the nonisothermal wall existing for the low-enthalpy heat-transfer measurements. The effect on boundary-layer development of this departure from an isothermal wall, while trivial for the case of the high-enthalpy shock-tunnel tests, was of some importance for the wind-tunnel tests. Estimates of the magnitude of this effect were made with the theory of reference 23. The results of these estimates indicate that heat-transfer coefficients measured on the top surface of the wind-tunnel model at $\alpha = 0^{\circ}$ may be as much as 30 percent higher than would be expected on an isothermal model. However, because of the various uncertainties involved in these calculations, the data were not adjusted for this effect.

A general trend noted in the longitudinal heating distributions is the difference in level of the two sets of data. The shock-tunnel distributions consistently lie below the wind-tunnel data with the greatest differences occurring on the surfaces least inclined to the stream. It is believed that this result is in accordance with the previous disscussions regarding the effects of Mach number, nonisothermal wall and the ratio of $\dot{q}/\dot{q}_o$ compared to h/h_o.

An additional point of interest noted in the wind-tunnel data is the area of high local heating which occurred on the upper surface of the nose. The level of heating in this area was about 20 percent in excess of the reference stagnation-point value. Good agreement was obtained with an estimate made with the theory of reference 24 and is seen in figure 5(b) as the cross symbol.

Circumferential heating distribution.- The circumferential distribution of heating at the approximate midpoint of the body is presented in figure 7. An estimated distribution is shown for $\alpha = 0^{\circ}$ in figure 7(a) and is found to lie between the two sets of data. This distribution was obtained by joining the heating rate values at $G/G_t = 0$ and 1 used in figure 5 with an estimated variation for a yawed cone and a swept cylinder.

Note in figure 7(b) that the wind-tunnel data for $\alpha = -14^{\circ}$ show a pronounced increase in heating on the upper curved leading edge. This edge approximates a portion of a swept cylinder. Despite the small radius of curvature, however, the heating of this region does not exceed that of the conical surface at $\alpha = 0^{\circ}$ which is approximately 40 percent of the reference stagnation value.

Body heating at angle of attack.- The influence of angle of attack on the heating distribution is illustrated in figure 8. Results obtained with the theory of reference 20 are shown for comparison with the data for the hemispherical and conical surfaces, and in figure 8(a), the data for the top surface are compared with estimates made with the theory of reference 21. It is seen that for the upper and lower meridians, agreement with the theoretical estimates is affected by body angle of attack. Note that the cone axis is parallel to the stream at $\alpha = -6.6^{\circ}$ and the top surface is parallel at $\alpha = 0^{\circ}$. As the body is pitched to positive angles of attack, the theoretical prediction falls increasingly below the results measured on the lower meridian, in both parts of figure 8

negative angles a similar trend is noted on the upper meridian in figure 8(a). Also note in figure 8(a) that heating of the upper nose area $(S'/r_o = 0.10)$, which was discussed with the longitudinal distributions as being greater than that of the stagnation point, steadily increases at negative angles of attack.

Control Heating

Body pressure field.- To assist in the analysis of the present measurements of control heating, a brief study was made of the flow fields in which the controls operate. In particular, pitot pressures were measured in the flow surrounding the body. These measurements were obtained from the wind-tunnel tests at M = 5 and the results are presented in figure 9. Note in figures 9(a) and 9(b) that the flow which passes through the normal portion of the bow shock wave and, hence, which has low pitot pressure is confined to a thin layer between the innermost impact tube and the conical surface. Indeed the pitot-pressure coefficients are relatively high; for example, at $\alpha = 0^o$ the pressure coefficient rises to about 4.8 at this location which is only 4 percent of the body diameter from the conical surface. This value approaches the theoretical maximum of about 5.2 which is attained at this Mach number by flow passing through the oblique portion of the bow shock and being isentropically compressed to the conical body surface.

It is seen in figure 9(c) for $\alpha = 0^o$ that all four pitot survey tubes were within the shock envelope at this Mach number and recorded pressures continuously increasing away from the body. At the body surface, the data approach the theoretical values for isentropic expansion of flow from the normal shock. Notice that the rate of pressure increase is much higher in this region at $\alpha = -14^o$; in fact, the pressures are tending to the level of those measured with the side and lower rakes.

Control set I.- Control set I consists of four flap-type controls attached to the rear of the body with a small gap between the control and the body surface. These controls, which are shown in figure 1(a), have an aspect ratio of 0.6 and were tested at deflection angles from 0^o to 80^o. For these controls, heating ratios are shown in figure 10 as a function of control deflection angle. The small triangular symbols represent locations at the aft inboard and outboard corners of the flap and the square symbols represent shock-tunnel data obtained at midchord near the edge. The bars on the wind-tunnel data represent the maximum and minimum values measured on the control at other locations. The flagged symbols in figures 10(b) and (c) are data obtained from shock-tunnel shots made at somewhat reduced enthalpy. They are, however, considered to be comparable with the data obtained at the nominal test condition.

The theoretical estimates of heating ratios for the trailing edge of the control in the wind-tunnel tests were obtained in the following manner. The flow was assumed to pass through the oblique shock wave of a 36.6^o half-angle cone, to proceed isentropically to the region of the control leading edge and

then to pass through the control shock wave; the control-shock-wave angles were determined from the shadowgraphs. A three-dimensional laminar boundary layer was assumed to begin at the control leading edge, and to be subjected to the control pressure distributions which were reported in reference 6. The theoretical estimates, shown in figure 10(a), are seen to lie between the two sets of measured values for the upper control and to be somewhat below the measurements for the lower control. The assumption of a boundary-layer origin at the control leading edge is believed to be the primary cause of the difference between the theory and data as the deflection angle is increased. Crossflow effects would be expected at the larger deflection angles with a consequent decrease in the local Reynolds number and an increase in the heating at the trailing edge of the control. The $\alpha = 0^{\circ}$ shock-tunnel data, seen in figure 10(b), show a continuous increase in heating with deflection angle at the midchord position. The heating for the trailing edge of both upper and lower controls, however, is relatively constant at deflection angles greater than about 40°.

The data presented in figure 10(c) show that at $\alpha = -14^{\circ}$ the upper control heating ratios are less in the shock tunnel than in the wind tunnel. At the higher Mach number of the shock tunnel the trailing edge of this control is believed to be outside the body shock-wave envelope. Theoretical estimates of the heating at the flap trailing edge are shown in figure 10(c) for $\alpha = -14^{\circ}$. These estimates are seen to be in fair agreement with the measured results in the wind tunnel. No means was found, however, to predict the very high heating at the forward edge of the control (indicated by the top of the bars) which is immersed in a complex flow field. Shadowgraphs of the flow about the model during the wind-tunnel tests at low enthalpy are seen in figure 11. Note the substantial differences in the flow over the upper control at 0° and -14° angles of attack.

An interesting result of a test in the shock tunnel indicates that the area of high heating at the forward edge of the control may extend onto the body surface. Figure 12(a) is a self-luminous photograph of flow over the model in the shock tunnel and figure 12(b) shows the model after test. The right-hand upper control was deflected 78° and the left-hand upper control was deflected 63°. Both controls were insulated from the model base and hence could not influence the top surface by thermal conduction. Notice in the photograph of the model after test the darkened oxidized areas on the top surface of the body directly in front of the controls. Unfortunately this area was not instrumented but a high local heating rate may certainly be inferred from the appearance of the model surface. Test results which were presented in reference 25 also indicate a substantial variation in the heating of the body surface in the vicinity of the controls.

Additional heating distributions measured in the wind tunnel for control set I are presented in figures 13 and 14. The data of these figures show that the highest heating generally occurred at the forward thermocouple location. Only three exceptions to this were found: the lower control at $\delta = 45^{\circ}$ for both angles of attack, and the upper control at $\delta = 10^{\circ}$ for $\alpha = 0^{\circ}$. A point of interest in the distributions for the upper control at $\alpha = 0^{\circ}$, figure 13(b),

the substantial spanwise heating gradients. Spanwise gradients are also displayed in the pressure data of reference 6 although at the rearmost station, $L/L_T = 0.9$, the pressure gradient is reversed with respect to the heating distribution.

The longitudinal heating distributions for control set I at 0° angle of attack are compared with theoretical predictions in figures 15 and 16. The theoretical curves were computed by the same method described with figure 10. The flow was assumed to pass through either the normal shock at the nose of the body or the oblique shock of a 36.6° half-angle cone as noted in the figures. Note that on the lower control (fig. 15), the longitudinal decrease in heat-transfer coefficients was found to be greater on the outer edge than on the inner edge. This trend is suggestive of a crossflow component away from the model center line which is consistent with the model geometry since at $\alpha = 0^\circ$ the cone axis is pitched 6.6°.

Control set II.- Heating distributions were measured in the wind tunnel with control set II for $\alpha = 0^\circ$ and -14°. A sketch of the model configuration is seen in figure 1(b). Note that the gap configuration is different from that used with control set I. A full-span open slot was obtained by straddle mounting the controls with extended tabs at the sides. The data, which are for $\delta = 25^\circ$ only, are in figure 17. Figure 18 is a shadowgraph of the flow at $\alpha = 0^\circ$. Note the close proximity to the body upper surface of the origin of the shock from the upper control. The gap configuration apparently limits boundary-layer separation at this deflection angle.

Relatively constant heating was found over the surface of these controls at both $\alpha = 0^\circ$ and -14°. The heating of the lower control decreases from about 60 percent to 30 percent of the reference stagnation value as the body is pitched from $\alpha = 0^\circ$ to -14°. The data for the yaw control, figure 17(b), show an average heating ratio of about 0.3 to 0.35 over most of the control at the two angles of attack and about 0.4 to 0.5 at the point nearest the body. The upper pitch control experienced approximately 1/3 of the heating of the lower control at $\alpha = 0^\circ$ and about equal heating at $\alpha = -14^\circ$. A curious spanwise heating gradient was noted at the station $L/L_t = 0.906$ of the upper control at $\alpha = -14^\circ$ (fig. 17(c)). Since the distribution on the same control was uniform at $\alpha = 0^\circ$, it is believed that a slight twisting of the control may have occurred as a result of the increased loads at $\alpha = -14^\circ$ inasmuch as the control was supported unsymmetrically.

Comparison of results for control set I and control set II.- Comparison of the heating ratios for the various flap controls is seen in figure 19. The longitudinal heating distributions measured in the wind tunnel are compared with estimates for three-dimensional laminar flow. The method used in making these estimates was described with figure 10. Flap pressures used for the estimates were the wind-tunnel measurements for control set I reported in reference 6.

Substantial differences in heating are noted between the two upper control configurations. The heat-transfer coefficients for the larger center control are roughly 1/2 those obtained on the outboard, lower aspect-ratio control.

(Comparison of results in figs. 14(b) and 17(c) shows that this is also true at $\alpha = -14^{\circ}$.) The deflection angles were not exactly the same, 25° as compared to 30°, but the primary cause of the difference is believed to be spanwise variations in the flow approaching the controls. The spanwise heating variations found on the upper control of set I (seen in figs. 13(b) and 14(b)) would further support this view. Note in figure 19(b) the similarity in the heating level of the two lower controls which are immersed in the conical flow from the body. The differences in heating between the lower and yaw control are attributed to the fact that this body attitude, $\alpha = 0^{\circ}$, requires the cone axis to be pitched 6.6°.

In view of the differences between the upper controls which may be largely due to their location with respect to the nonuniform flow field generated by the forebody, and the lack of difference in the two lower controls, which may be associated with the small deflection angle used in the test, it is believed that conclusions regarding the effects of flap aspect ratio and gap configuration must await a more extensive investigation.

Elevons.- Small elevonlike controls, tested in the 10- by 14-inch wind tunnel, are sketched in figure 1(c). Representative heating ratios measured on the leading edge and on the upper and lower surfaces of these controls are shown in figures 20 and 21. Heating of the leading edge is seen to vary from about 0.6 to 0.8 of the reference stagnation value and heating ratios for the upper and lower surfaces are in the range from 0.1 to about 0.4. In figure 20 the leading-edge heating is compared with estimates obtained with the ideal-gas swept-cylinder theory of reference 26. Theoretical estimates are shown for three types of flow. For two of the estimates a Prandtl-Meyer expansion was assumed to originate at the rear edge of the body and to continue until the resulting Mach line and the leading edge of the elevon were coincident; the leading edge of the elevon was considered to be a swept cylinder in the resulting flow field to obtain the estimated heat-transfer coefficients. In one estimate the conditions at the rear edge of the forebody were for a normal forebody shock and in the other for an oblique shock. The leading-edge data are somewhat below the theoretical value obtained assuming normal shock total head for the unpitched cone ($\alpha = -6.6^{\circ}$) and exhibit a nearly symmetrical increase in heating with cone pitch angle. For the upper and lower elevon surfaces the trend of the data is as expected: the lower surface heating increases with nose-up body pitch angle and the upper surface heating decreases. Although the lower surface data are somewhat erratic, approximately equal heating of the upper and lower surfaces did occur when the cone axis was alined with the free stream ($\alpha = -6.6^{\circ}$).

Elevon heating as a function of deflection angle at three angles of attack is presented in figure 21. The relative insensitivity of the leading-edge heating to control deflection angle may be indicative of heat conduction in the elevon skin. Estimates of the magnitude of this effect, however, yielded an estimated error of less than 10 percent.

Base heating.- Base-heating measurements of an exploratory nature were made in the present investigation. Heat-transfer coefficients obtained for the base of the wind-tunnel model are presented in figure 22. Two models were used for these tests. The first, sketched in figure 1(d), was supported by a dual sting attached to the model at the location of the upper controls and the second was

upported in the conventional manner with a single central sting. The data obtained with the top supported model, figures 22(a), (b), and (c), exhibit a marked decrease in heating from the edge of the base to the center. This distribution as seen in figure 22(a) is symmetrical with the lower flaps removed and varies from about 4 percent to 1 percent of the reference stagnation-point value. Considerable asymmetry in the heating distribution occurred with the lower controls undeflected (fig. 22(b)). It is believed that this asymmetry may have resulted from a nonexact alinement of the small controls with the surface of the body. In figure 22(c) it is seen that heating ratios of approximately 8 percent were measured near the edge of the base. The data of the sting supported model (fig. 22(d)) suggest relatively uniform base heating, but for the three locations at which measurements were made with both support systems, the heating ratios are the same as in figure 22(b). It should be noted that the same dual support system as in the present tests was used for the measurement of base pressures (ref. 6). These measurements showed rather constant pressures over the base, in contrast to the present measurements which show a significant decrease in heating toward the base center. It is indicated, therefore, that the observed variations in heating are not due to variations in pressure but to some other phenomenon.

CONCLUDING REMARKS

The aerodynamic heating of a blunt lifting body with controls has been investigated experimentally. Measurements were made at a Mach number of 5 and a stream stagnation enthalpy of 160 Btu/lb in a steady-flow wind tunnel and at a Mach number of 10 and a stream stagnation enthalpy of 4000 Btu/lb in a combustion-driven shock tunnel. The stream Reynolds numbers based on body diameter were 0.72×10^6 and 0.012×10^6, respectively. Results were obtained for angles of attack from $+6.5^\circ$ to -14° and for three control configurations. Analysis of the results has shown the following:

1. Heating distributions measured on the nose and conical surfaces of the body were similar at the two enthalpy levels and could be predicted by theory.

2. Heating distributions measured in the two facilities on the flat upper surface were dissimilar. The data for higher Mach number and enthalpy from the shock tunnel indicated somewhat lower heating relative to the stagnation point.

3. Control surfaces extending into the flow field generated by the blunt asymmetrical forebody shape encounter a local stream of relatively high total head. At large deflection angles the controls are subjected to heating considerably in excess of that at the stagnation point of the body. There was some indication that the heating of adjacent areas of the body also was high.

4. Heating of the upper flap controls depended on their lateral location on the body. The center-mounted control received approximately one half of the heating experienced by outboard mounted controls.

[redacted]

5. Heating of the leading edge of small elevonlike controls mounted at the rear of the body was approximately 70 percent of body stagnation heating and was in general agreement with swept-cylinder theory.

6. Wind-tunnel measurements of base heating reveal a pronounced increase in heating at the outer edge of the base relative to that at the center. This is in contrast to pressure measurements which show essentially uniform base pressures.

Ames Research Center
National Aeronautics and Space Administration
Moffett Field, Calif., Nov. 12, 1962

[redacted]

[redacted]

REFERENCES

1. Eggers, Alfred J., Jr.: The Possibility of a Safe Landing. Space Technology, Ch. 13, Howard S. Seifert, ed., John Wiley and Sons, Inc., New York, 1959, pp. 13-01 to 13-53.

2. Chapman, Dean R.: An Approximate Analytical Method for Studying Entry Into Planetary Atmospheres. NASA TR R-11, 1959 (Supersedes NACA TN 4276).

3. Wong, Thomas J., and Slye, Robert E.: The Effect of Lift on Entry Corridor Depth and Guidance Requirements for the Return Lunar Flight. NASA TR R-80, 1961.

4. Slye, Robert E.: An Analytical Method for Studying the Lateral Motion of Atmosphere Entry Vehicles. NASA TN D-325, 1960.

5. Eggers, Alfred J., Jr., and Wong, Thomas J.: Re-entry and Recovery of Near-Earth Satellites, With Particular Attention to a Manned Vehicle. NASA MEMO 10-2-58A, 1958.

6. Sarabia, Michael F.: Aerodynamic Characteristics of a Blunt Half-Cone Entry Configuration at Mach Numbers From 3 to 6. NASA TM X-393, 1960.

7. Dennis, David H., and Edwards, George G.: The Aerodynamic Characteristics of Some Lifting Bodies. NASA TM X-376, 1960.

8. Savage, Howard E., and Tinling, Bruce E.: Subsonic Aerodynamic Characteristics of Several Blunt, Lifting, Atmospheric-Entry Shapes. NASA MEMO 12-24-58A, 1959.

9. Hassell, James L., Jr.: Investigation of the Low-Subsonic Stability and Control Characteristics of a 1/3-Scale Free-Flying Model of a Lifting-Body Reentry Configuration. NASA TM X-297, 1960.

10. Reller, John O., Jr., and Seegmiller, H. Lee: Convective Heat Transfer to a Blunt Lifting Body. NASA TM X-378, 1960.

11. Tunnell, Phillips J.: The Static and Dynamic Stability Derivatives of a Blunt Half-Cone Entry Configuration at Mach Numbers From 0.70 to 3.50. NASA TM X-577, 1961.

12. DeRose, Charles E.: The Aerodynamic Characteristics of a Blunt Half-Cone Entry Configuration Obtained From Ballistic-Range Tests at Mach Numbers Near 3. NASA TM X-578, 1961.

13. Holtzclaw, Ralph W.: Static Stability and Control Characteristics of a Half-Cone Entry Configuration at Mach Numbers From 2.2 to 0.7. NASA TM X-649, 1962.

[redacted]

14. McDevitt, John B., and Mellenthin, Jack A.: Characteristics of a Blunt Half-Cone Entry Configuration at Mach Numbers From 10.9 to 21.2 in Helium. NASA TM X-655, 1962.

15. Eggers, Alfred J., Jr., and Nothwang, George J.: The Ames 10- by 14-Inch Supersonic Wind Tunnel. NACA TN 3095, 1954.

16. Cunningham, Bernard E., and Kraus, Samuel: A 1-Foot Hypervelocity Shock Tunnel in Which High-Enthalpy, Real-Gas Air Flows Can Be Generated With Flow Times of About 180 Milliseconds. NASA TN D-1428, 1962.

17. Wolfe, G. W., and Arne, V. L.: Thermal Properties of Solids. Rep. E9R-12073, Chance Vought Aircraft, Oct. 13, 1959.

18. Stine, Howard A., and Wanlass, Kent: Theoretical and Experimental Investigation of Aerodynamic-Heating and Isothermal Heat-Transfer Parameters on a Hemispherical Nose With Laminar Boundary Layer at Supersonic Mach Numbers. NACA TN 3344, 1954.

19. Fay, J. A., and Riddell, F. R.: Theory of Stagnation Point Heat Transfer in Dissociated Air. Jour. Aero. Sci., vol. 25, no. 2, Feb. 1958, pp. 73-85, 121.

20. Lees, Lester: Laminar Heat Transfer Over Blunt-Nosed Bodies at Hypersonic Flight Speeds. Jet Propulsion, vol. 26, no. 4, April 1956, pp. 259-269, 274.

21. Van Driest, E. R.: The Laminar Boundary Layer With Variable Fluid Properties. Rep. No. AL-1855, North American Aviation, Inc., Jan. 19, 1954.

22. Romig, Mary F., and Dore, F. J.: Solutions of the Compressible Laminar Boundary Layer Including the Case of a Dissociated Free Stream. Rep. ZA-7-012, CONVAIR, Aug. 4, 1954.

23. Chapman, Dean R., and Rubesin, Morris W.: Temperature and Velocity Profiles in the Compressible Laminar Boundary Layer With Arbitrary Distribution of Surface Temperature. Jour. Aero. Sci., vol. 16, no. 9, Sept. 1949., pp. 547-565.

24. Reshotko, Eli: Heat Transfer to a General Three-Dimensional Stagnation Point. Jet Propulsion, vol. 28, no. 1, Jan. 1958., pp. 58-60.

25. Holdaway, George H., Polek, Thomas E., and Kemp, Joseph H., Jr.: Aerodynamic Characteristics of a Blunt Half-Cone Entry Configuration at Mach Numbers of 5.2, 7.4, and 10.4. NASA TM X-782, 1963.

26. Goodwin, Glen: Heat-Transfer Characteristics of Blunt Two- and Three-Dimensional Bodies at Supersonic Speeds. NACA RM A55L13a, 1956.

TABLE I.- COMPARISON OF MEASURED EQUILIBRIUM WALL TEMPERATURE AND THEORETICAL ADIABATIC WALL TEMPERATURES

$\alpha = 0^{\circ}$

$\frac{S'}{r_o}$	T_{EW}, °F (measured)	T_{AW}, °F (ref. 18)
Upper surface meridian		
1.875	150	142
1.372	152	143
.873	156	143
.425	178	178
.104	188	197
Lower surface meridian		
.187	197	199
.573	193	192
1.025	191	177
2.194	173	174
3.352	180	176

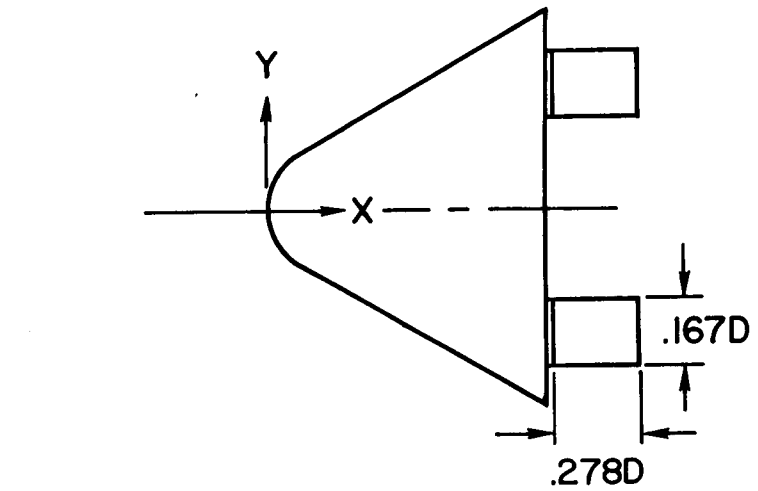

X/D	Y/D
0	0
.012	.068
.022	.090
.036	.110
.056	.133
.078	.152
.111	.176
.156	.205
.200	.231

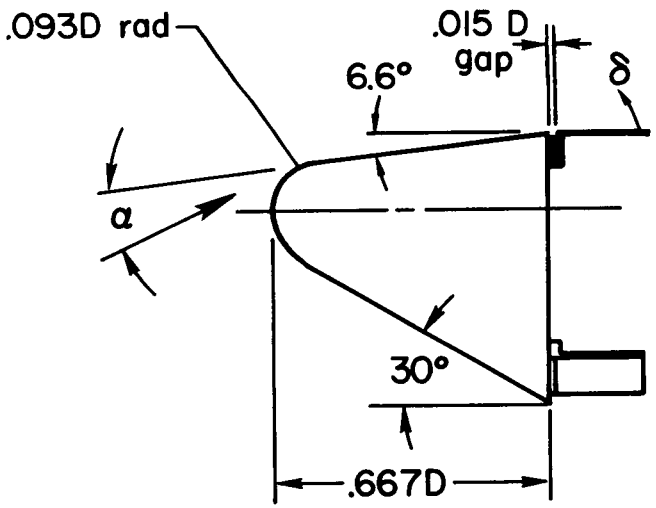

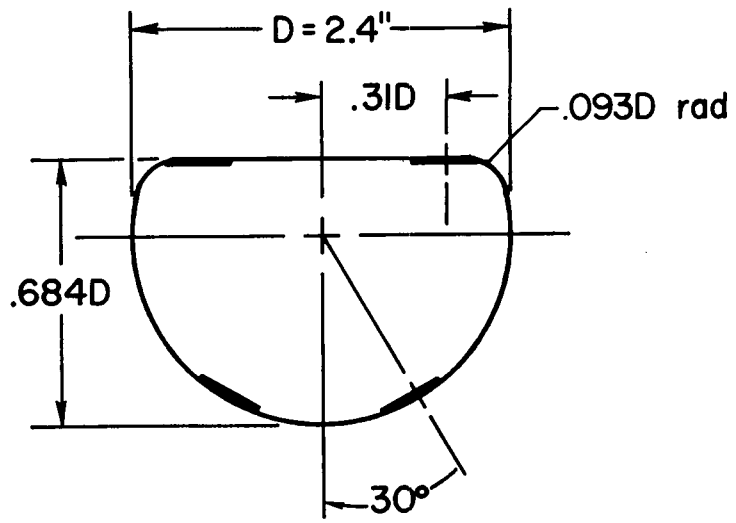

(a) Control set I.

Figure 1.- Sketch of test model with various controls.

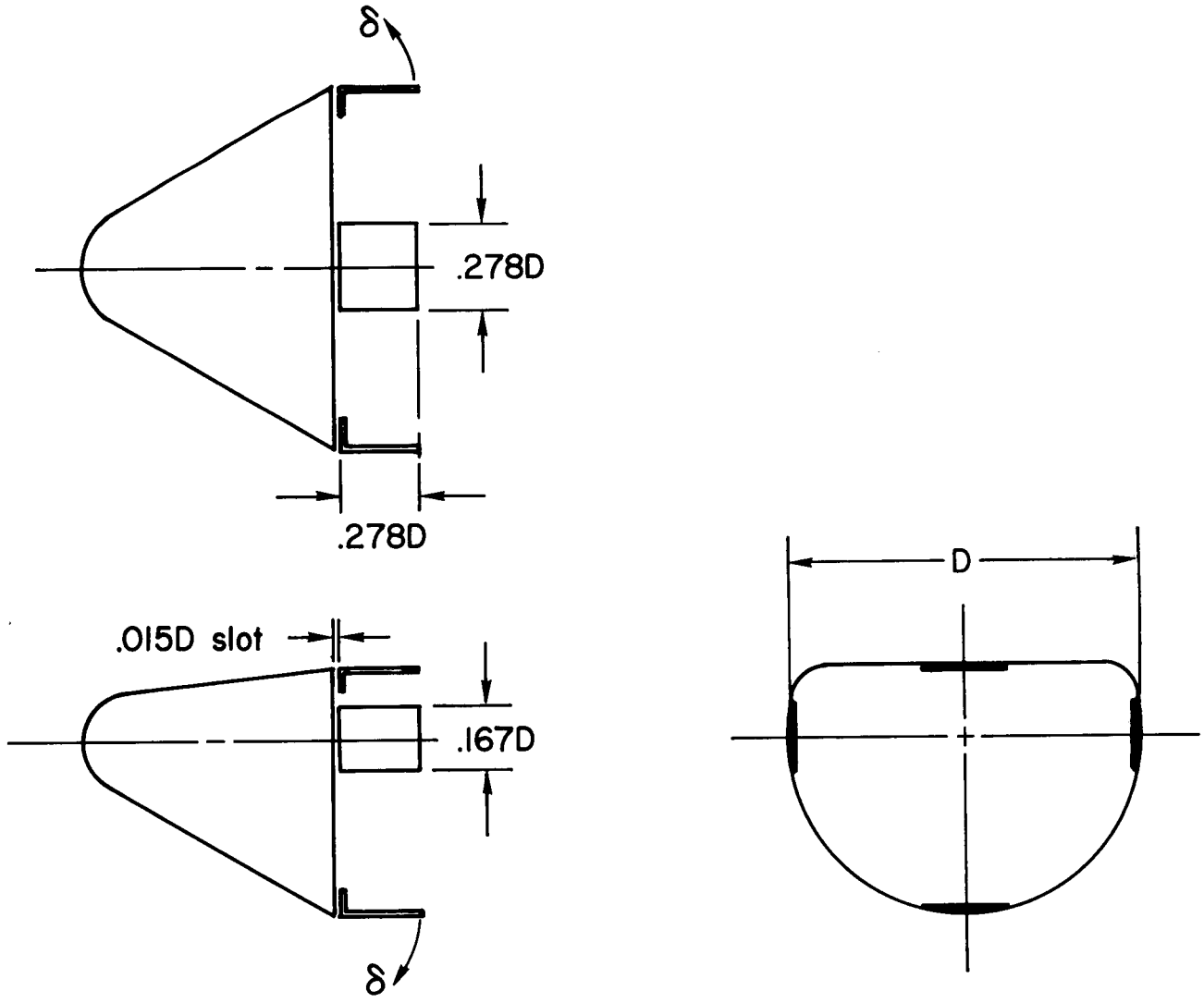

(b) Control set II.

Figure 1.- Continued.

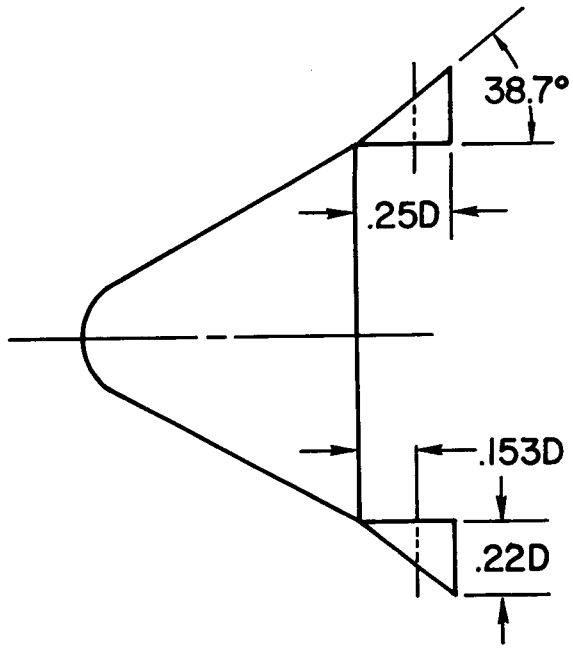

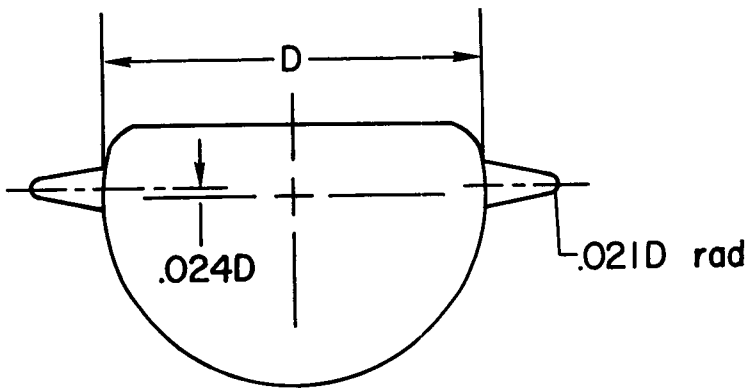

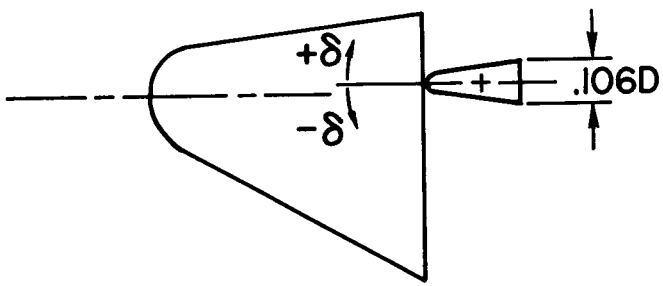

(c) Elevon controls.

Figure 1.- Continued.

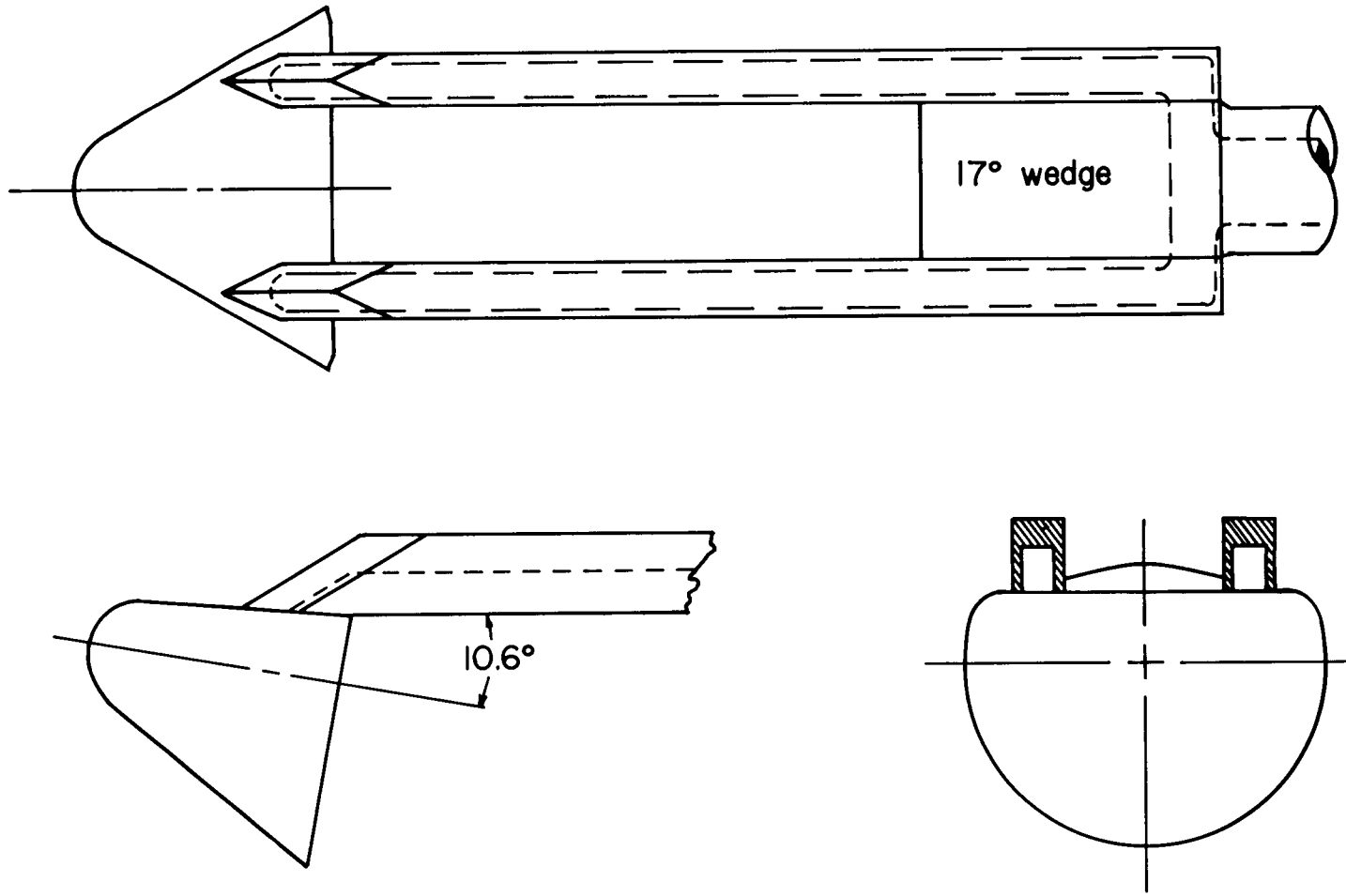

(d) Top support.

Figure 1.- Concluded.

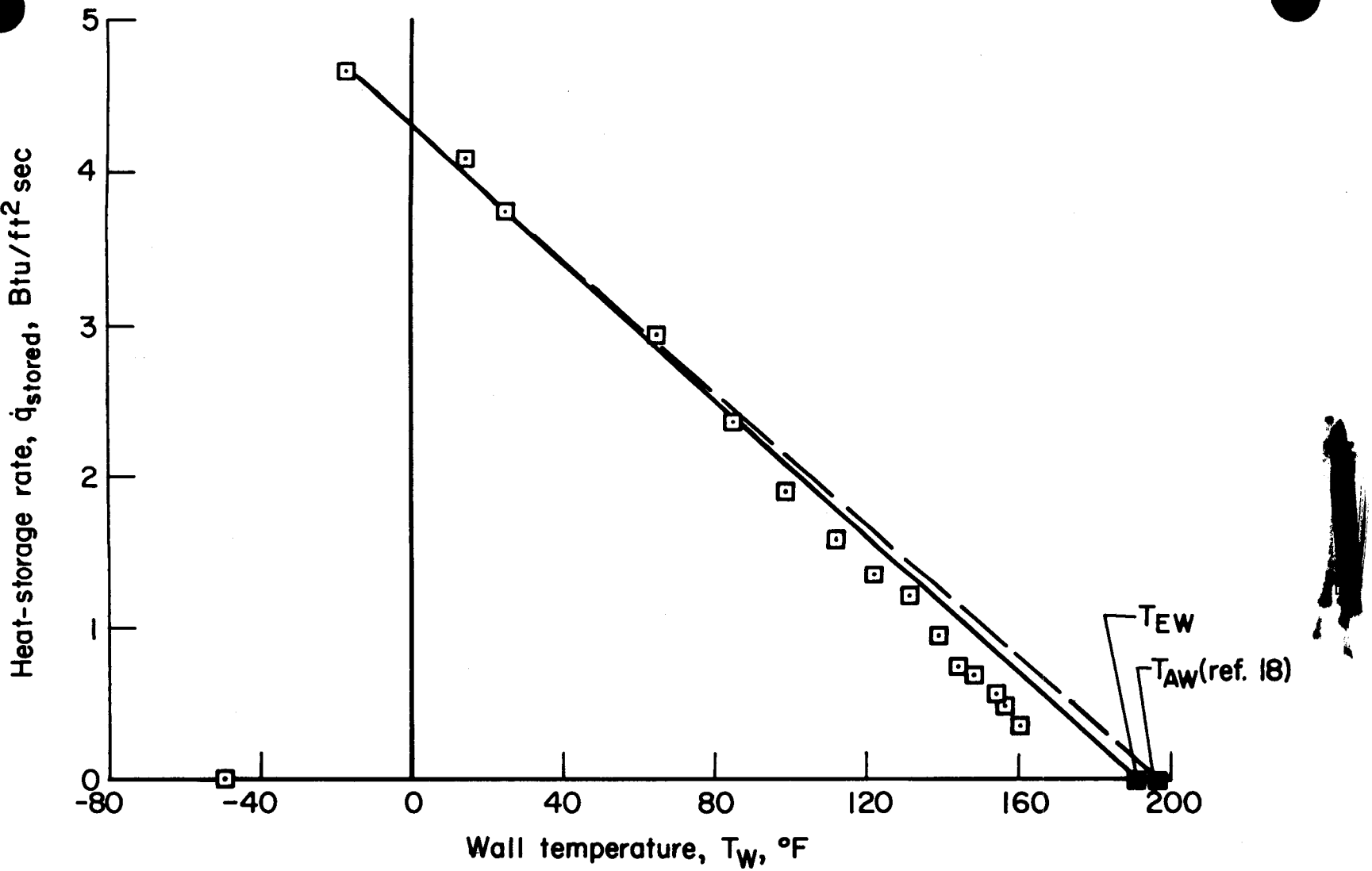

(a) Heat storage rate.

Figure 2.- Variation of heating data with wall temperature in the wind tunnel for the lower surface meridian at $S'/r_o = 0.57$; $\alpha = 0^o$.

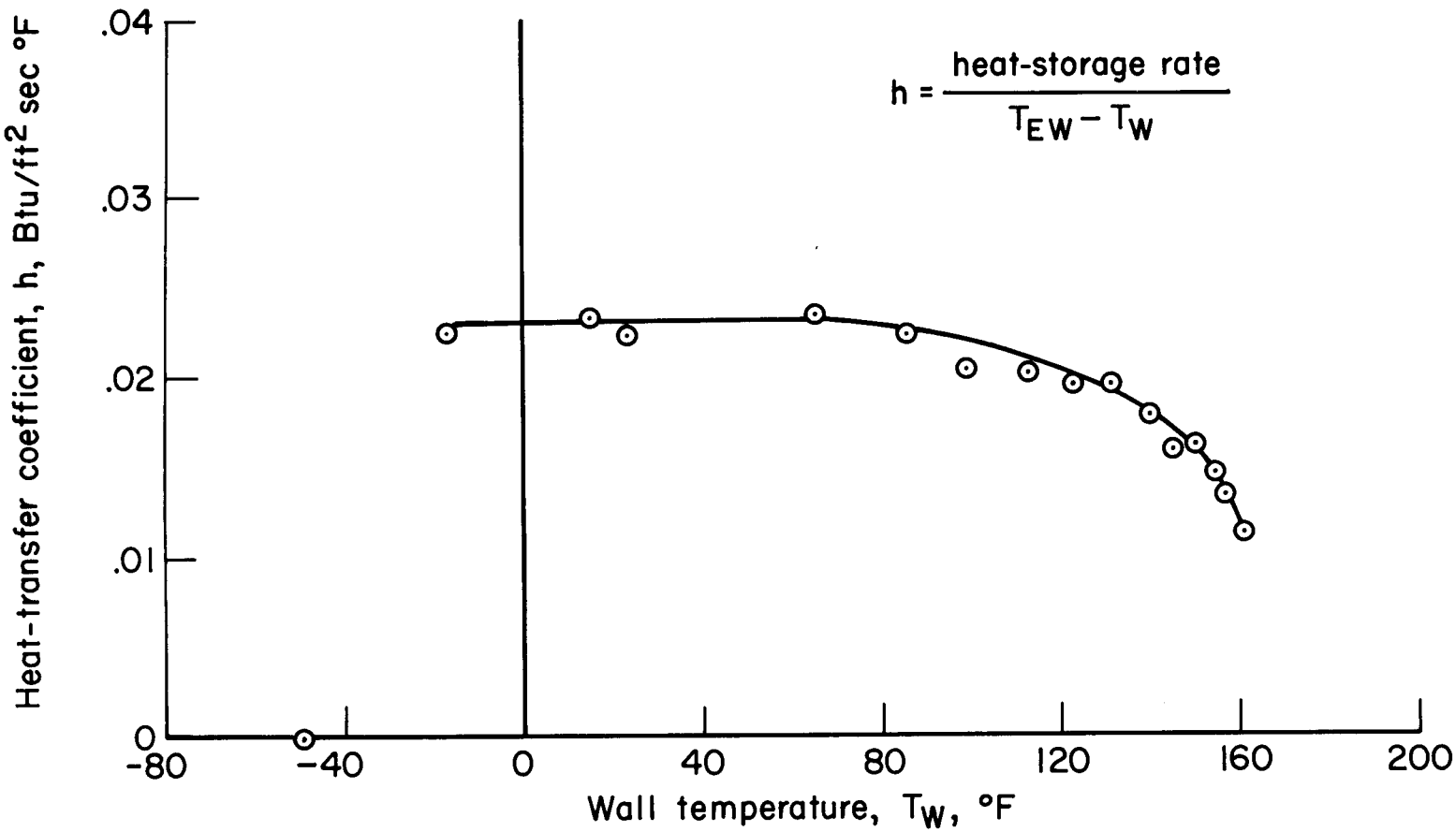

(b) Heat-transfer coefficient.

Figure 2.- Concluded.

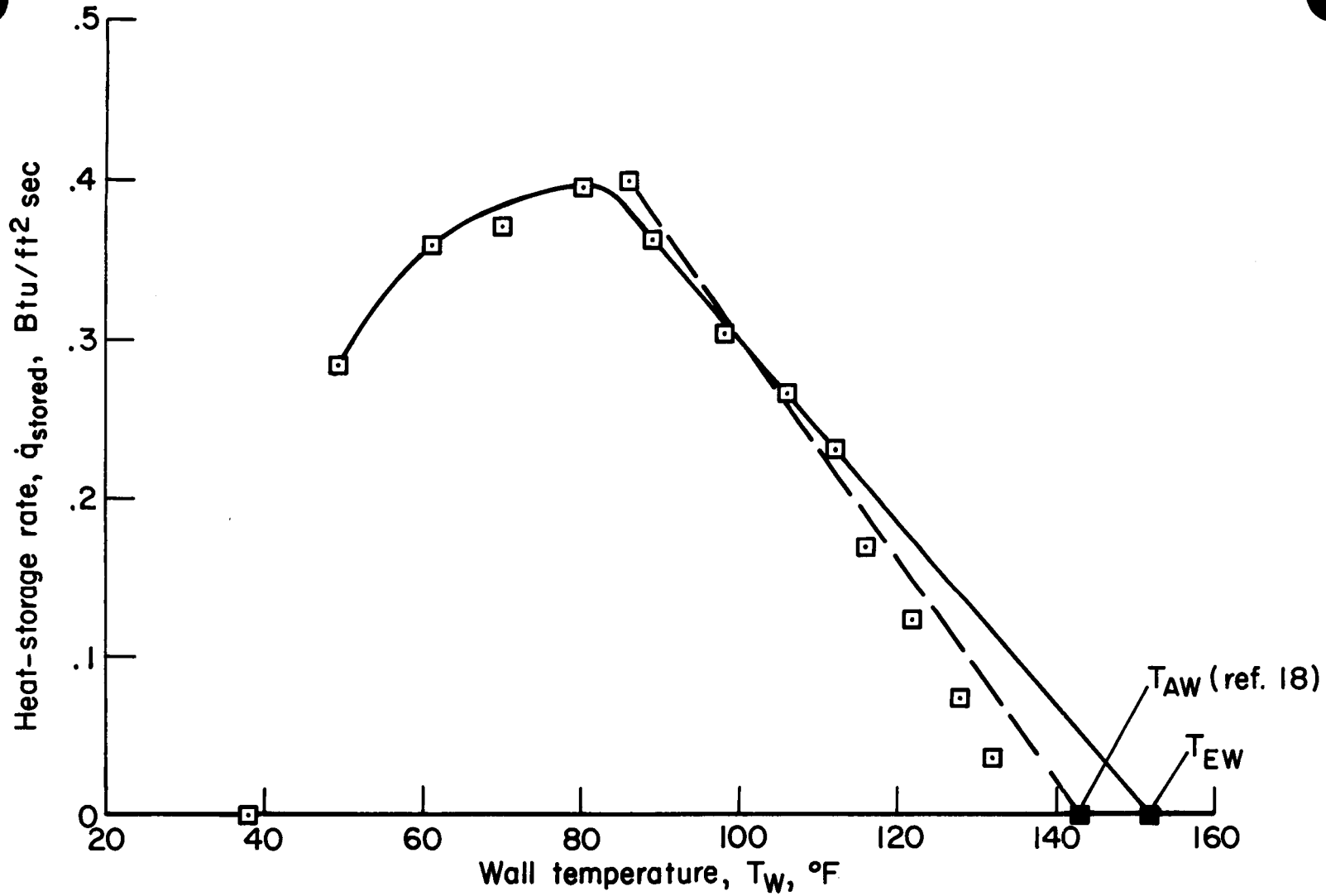

(a) Heat storage rate.

Figure 3.- Variation of heating data with wall temperature in the wind tunnel for the upper surface meridian at $S'/r_o = 1.37$; $\alpha = 0^o$ (controls off).

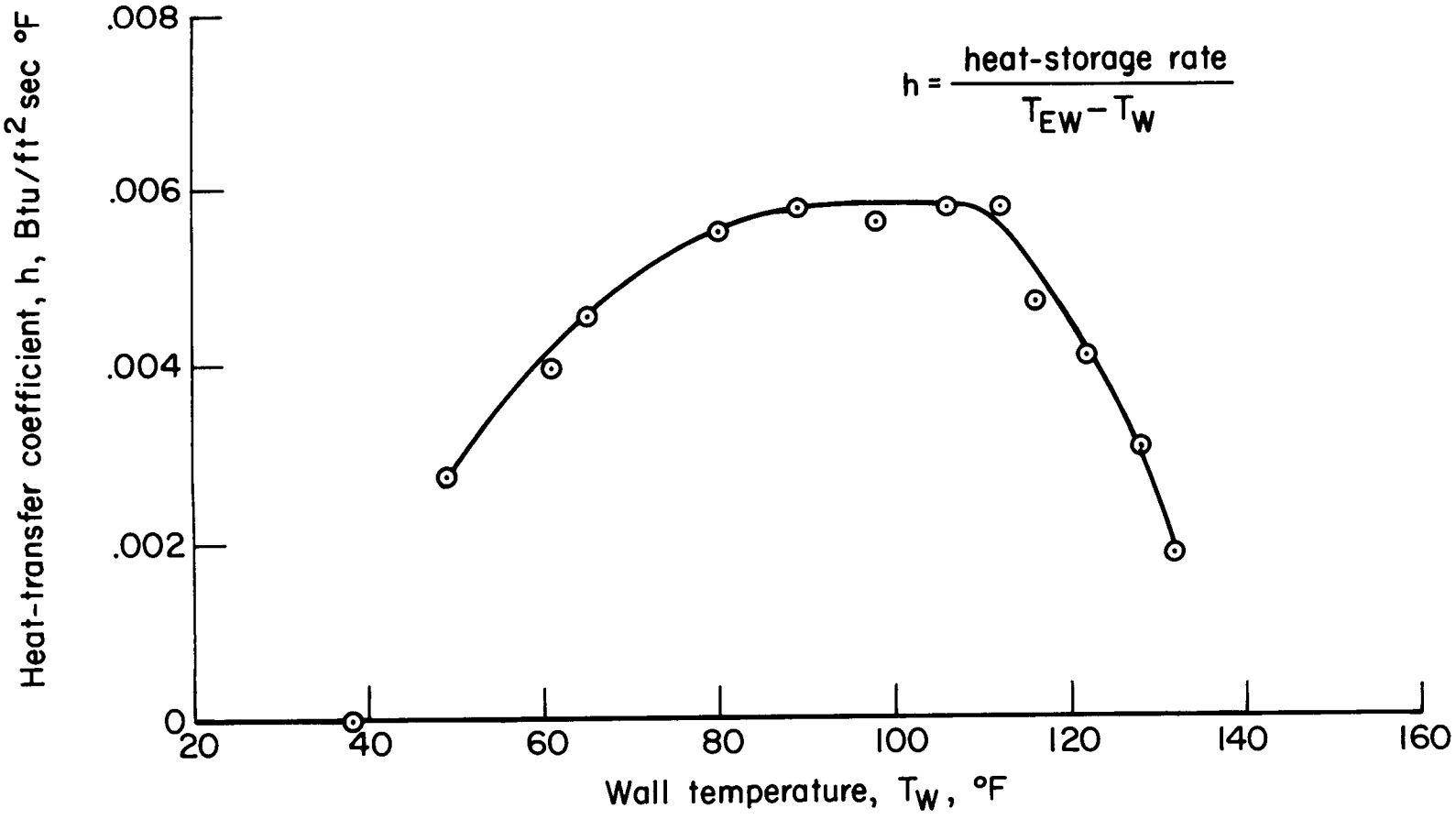

(b) Heat-transfer coefficient.

Figure 3.- Concluded.

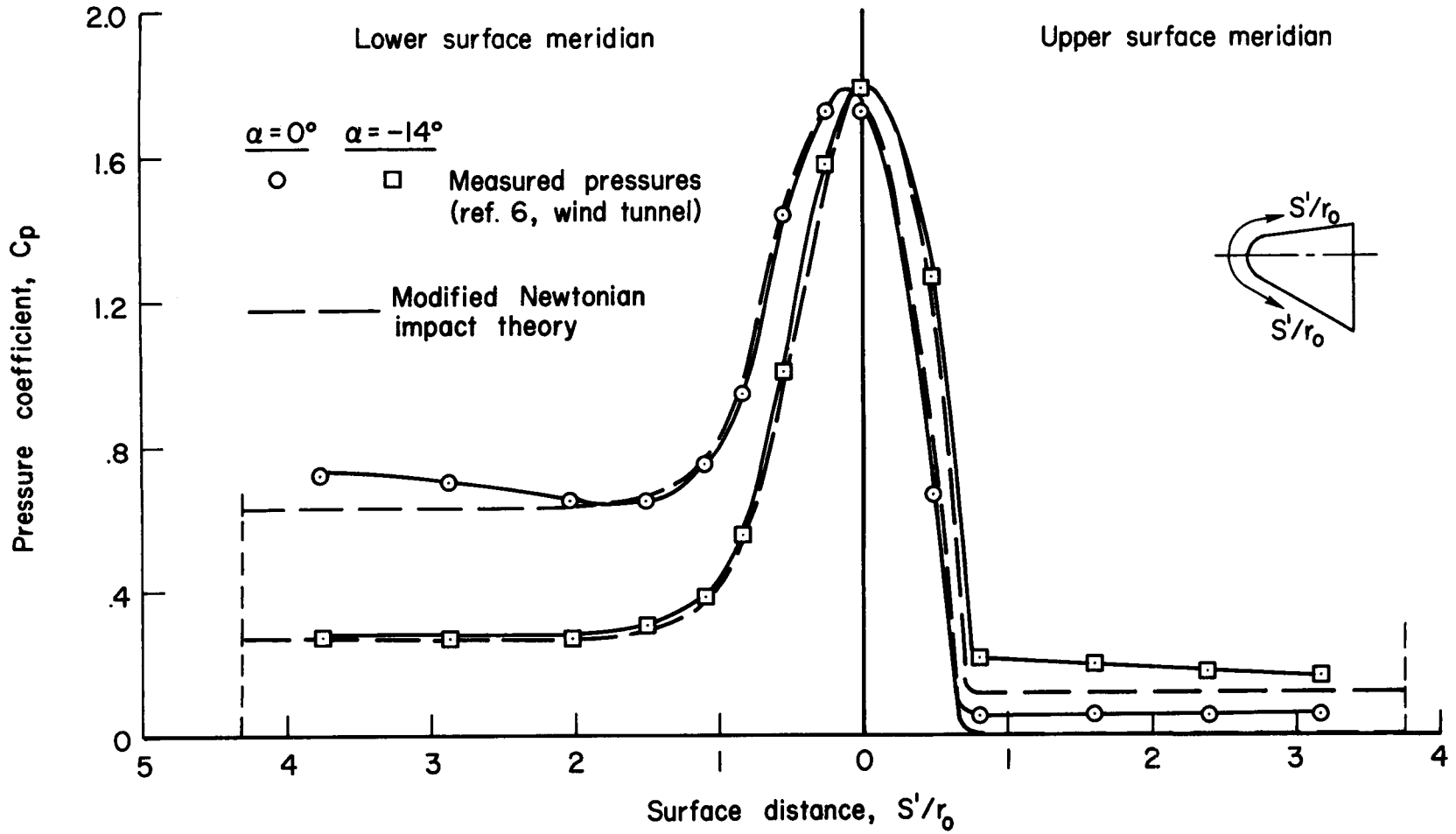

Figure 4.- Longitudinal body pressure distributions measured in the wind tunnel.

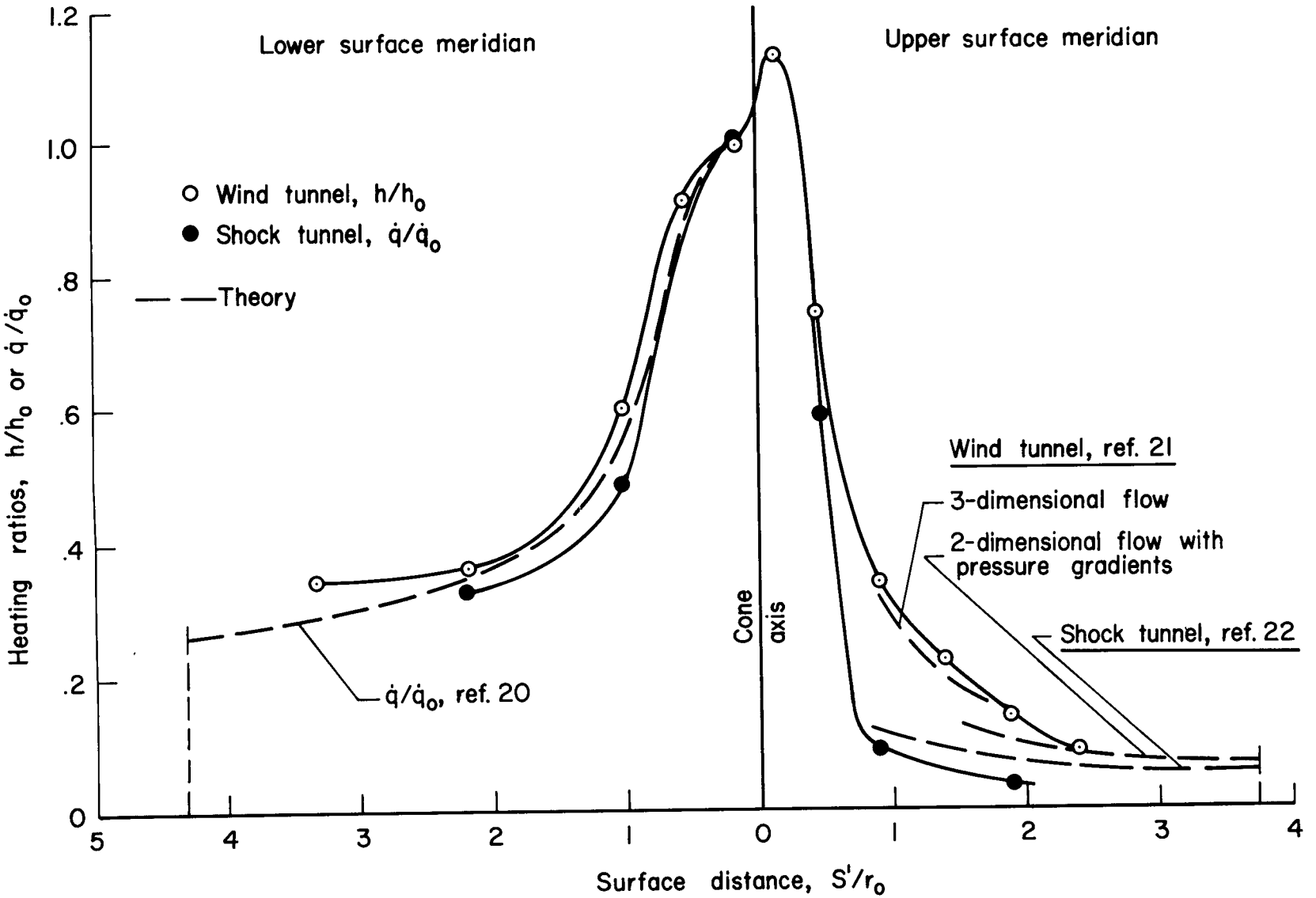

(a) $\alpha = 0^\circ$

Figure 5.- Comparison of longitudinal heating distributions measured in the wind tunnel and the shock tunnel.

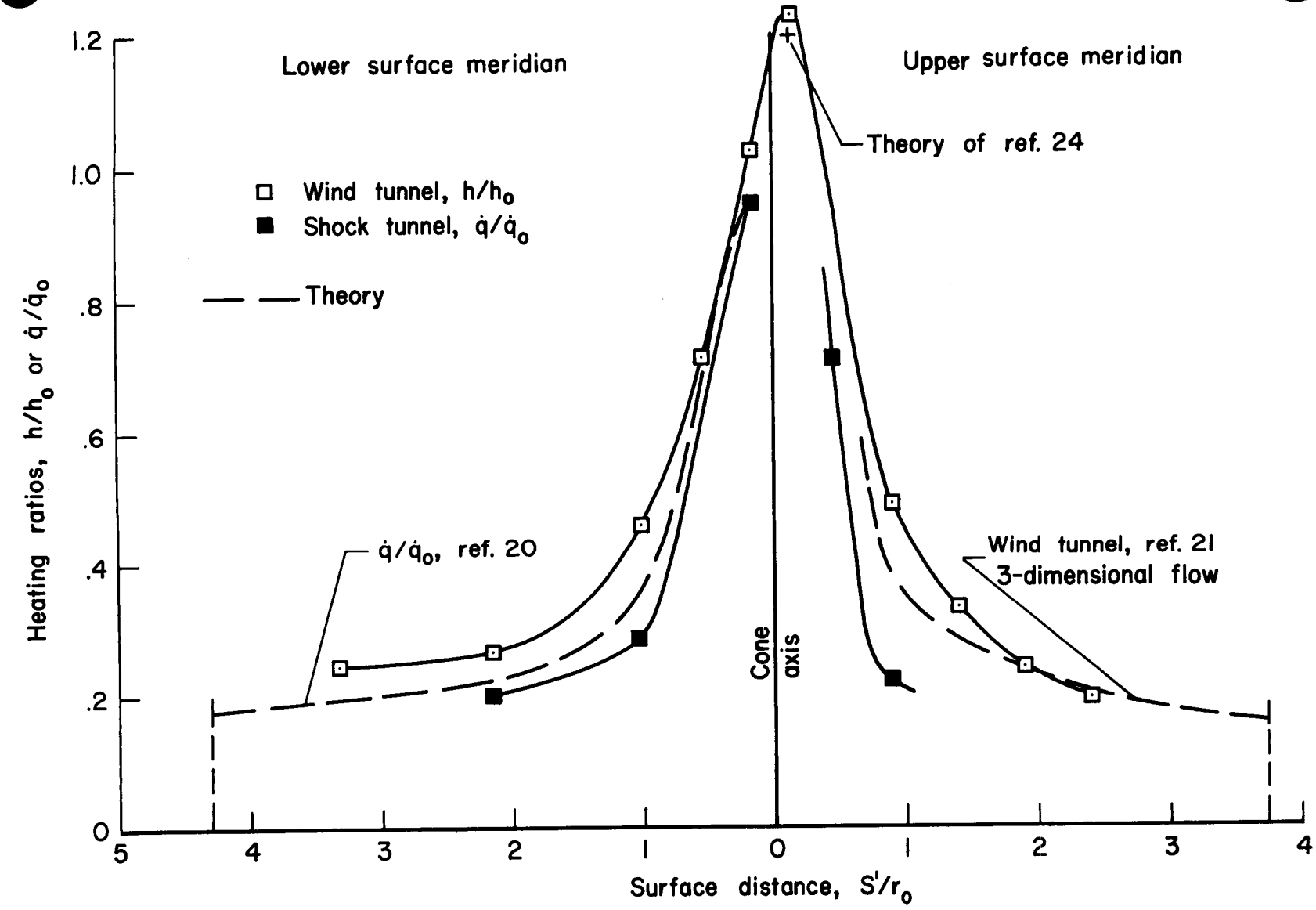

(b) $\alpha = -14^{\circ}$

Figure 5.- Concluded.

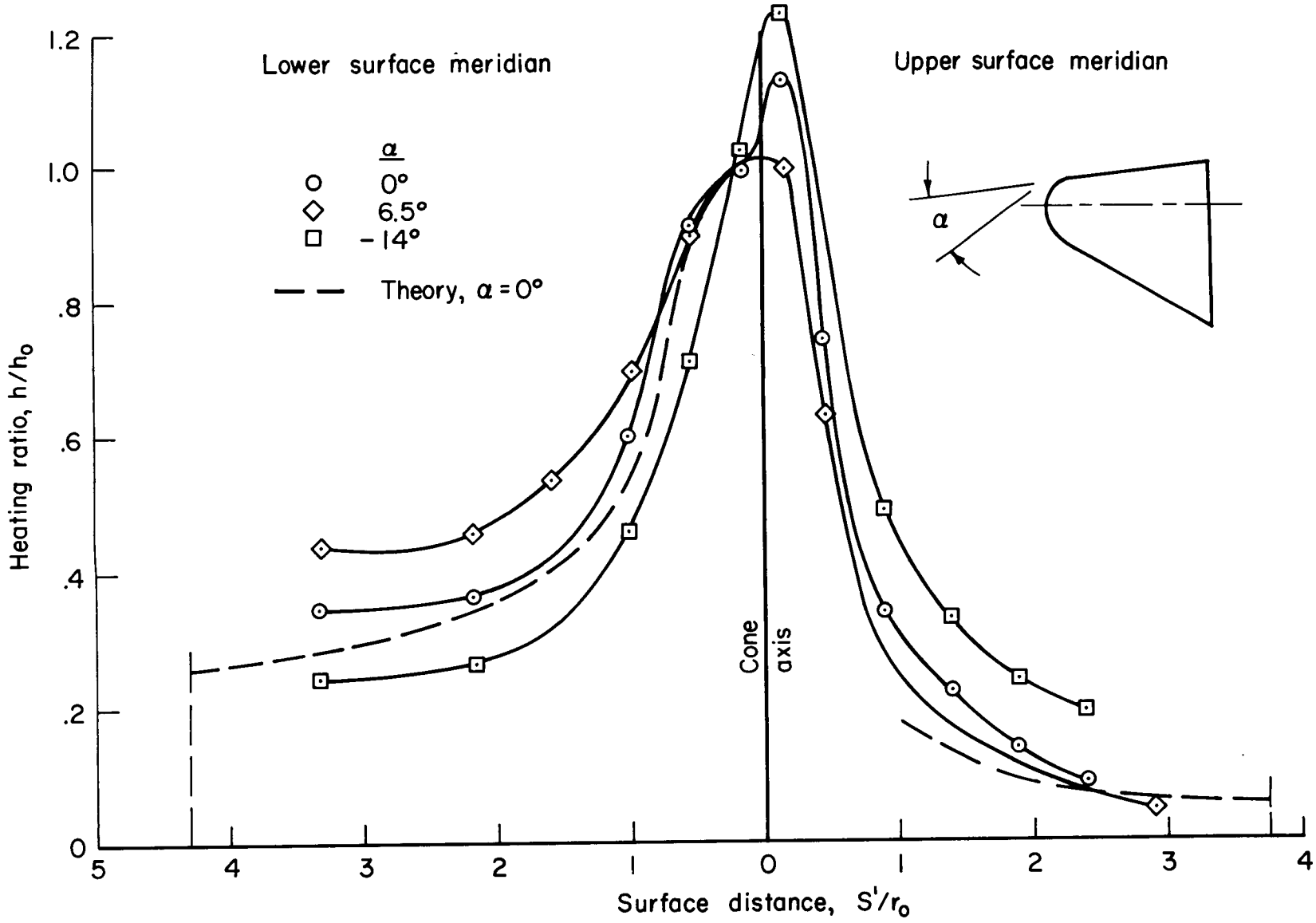

(a) Wind tunnel.

Figure 6.- Variation of longitudinal heating distributions with angle of attack.

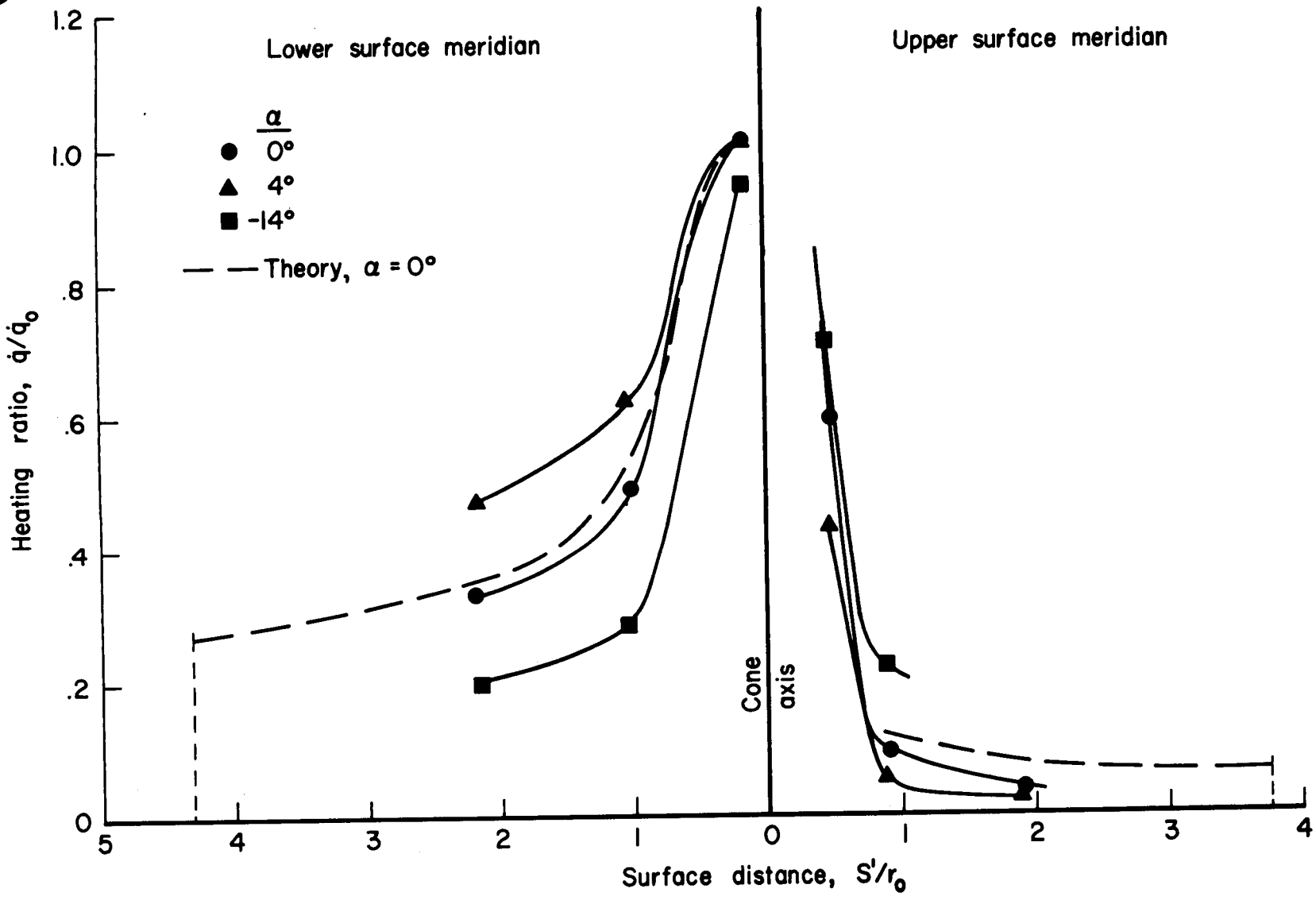

(b) Shock tunnel.

Figure 6.- Concluded.

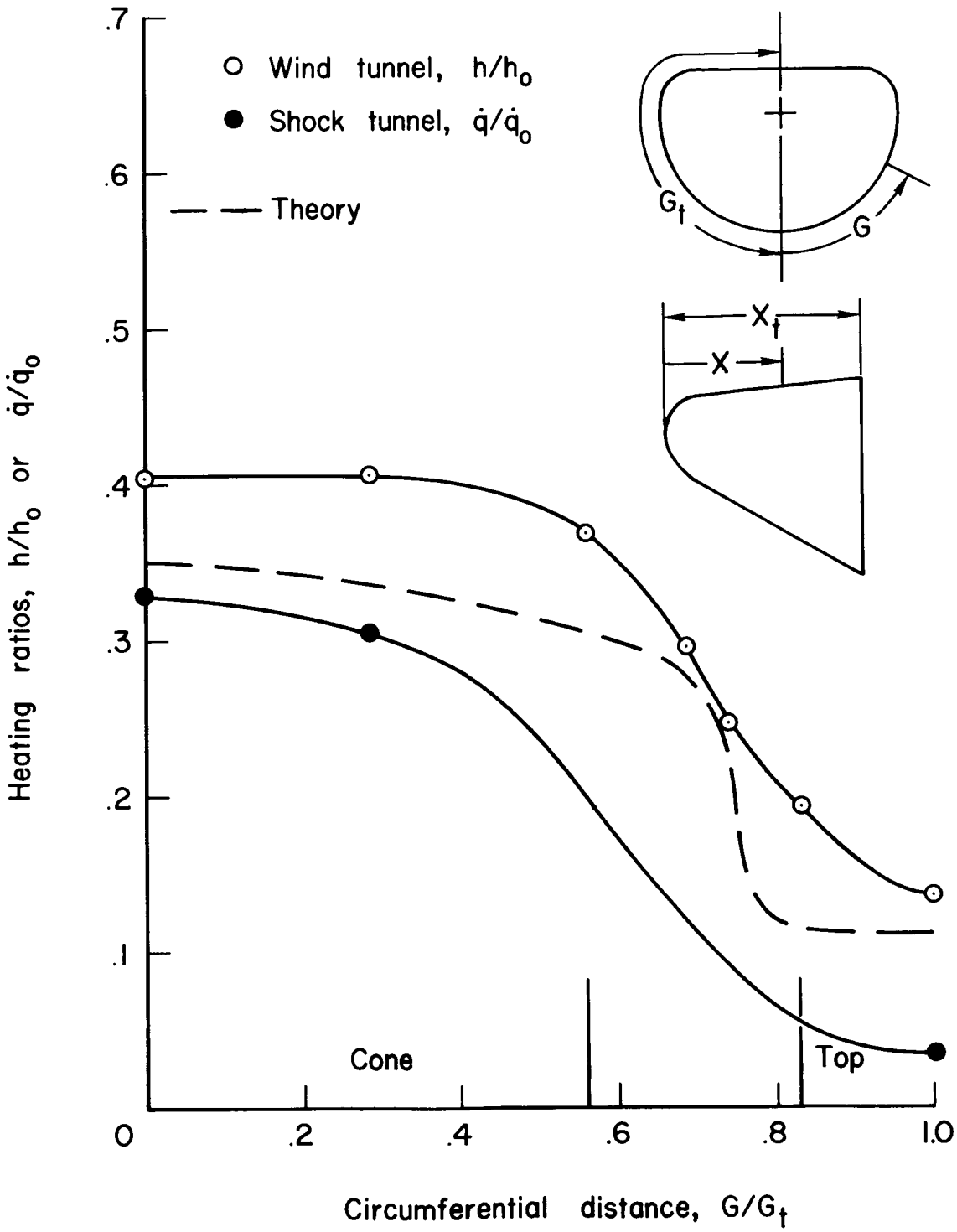

(a) $\alpha = 0^\circ$

Figure 7.- Circumferential heating distributions at $X/X_t = 0.45$ for three angles of attack.

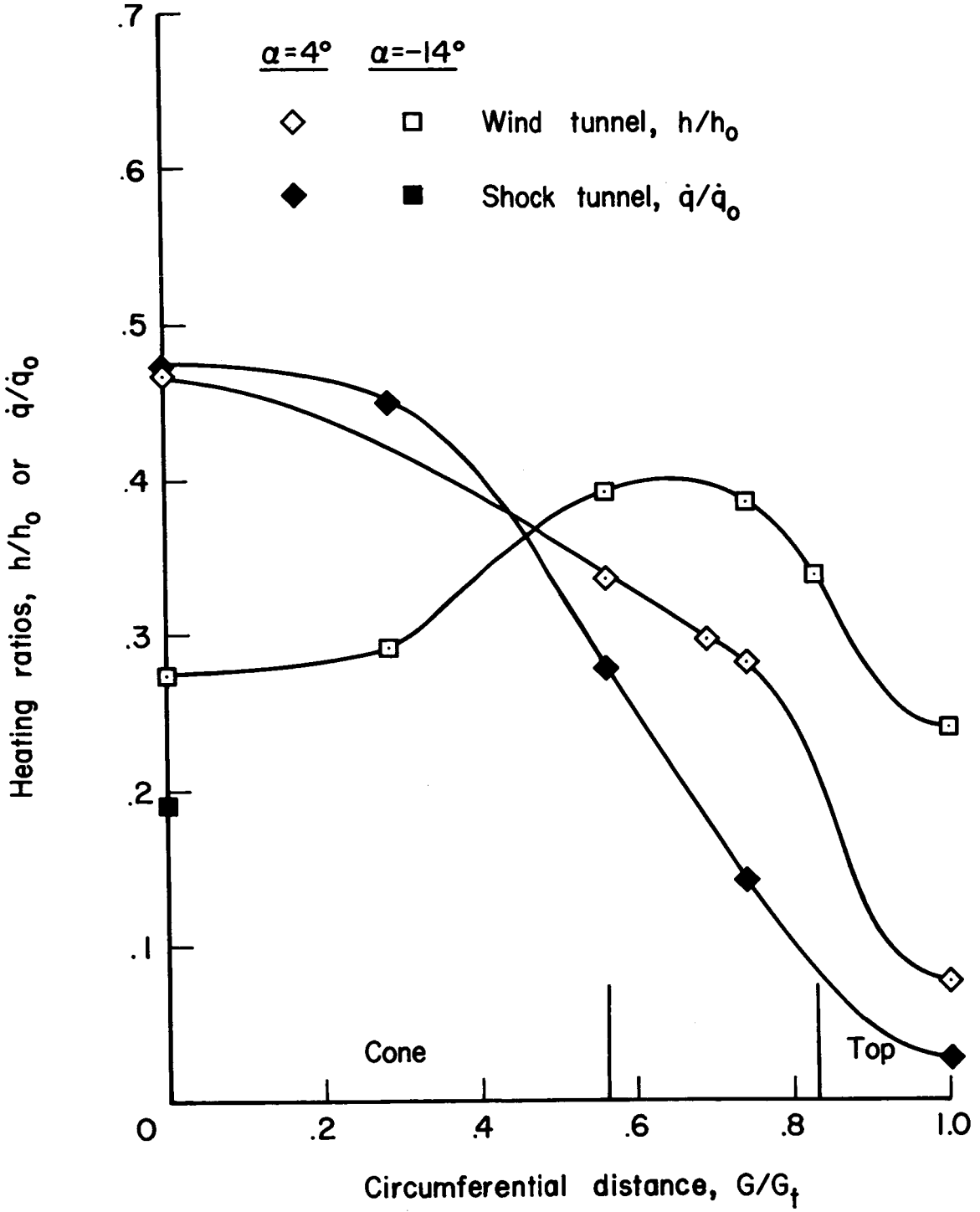

(b) $\alpha = 4^{\circ}, -14^{\circ}$

Figure 7.- Concluded.

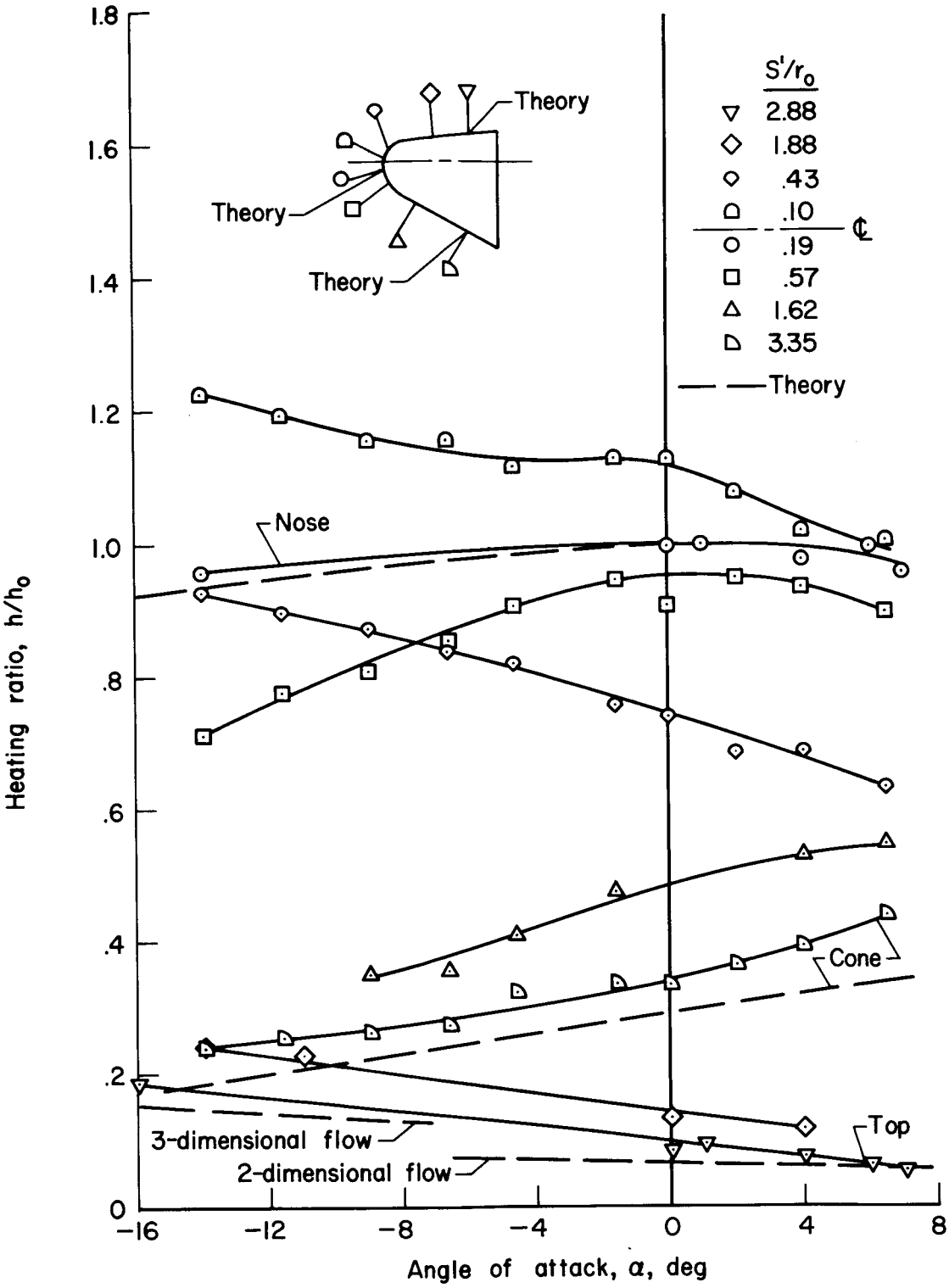

(a) Wind tunnel.

Figure 8.- Variation of body heating with angle of attack.

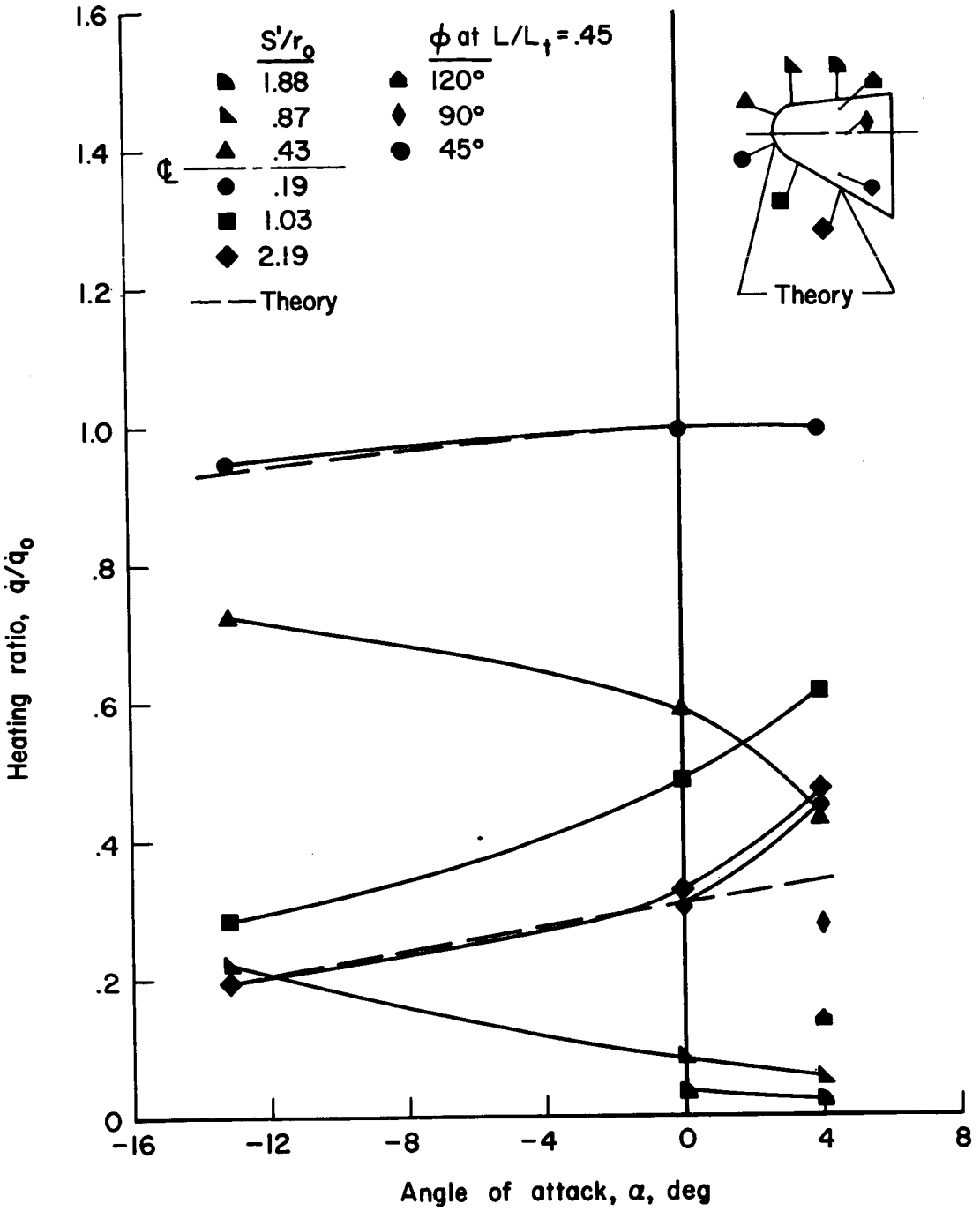

(b) Shock tunnel.

Figure 8.- Concluded.

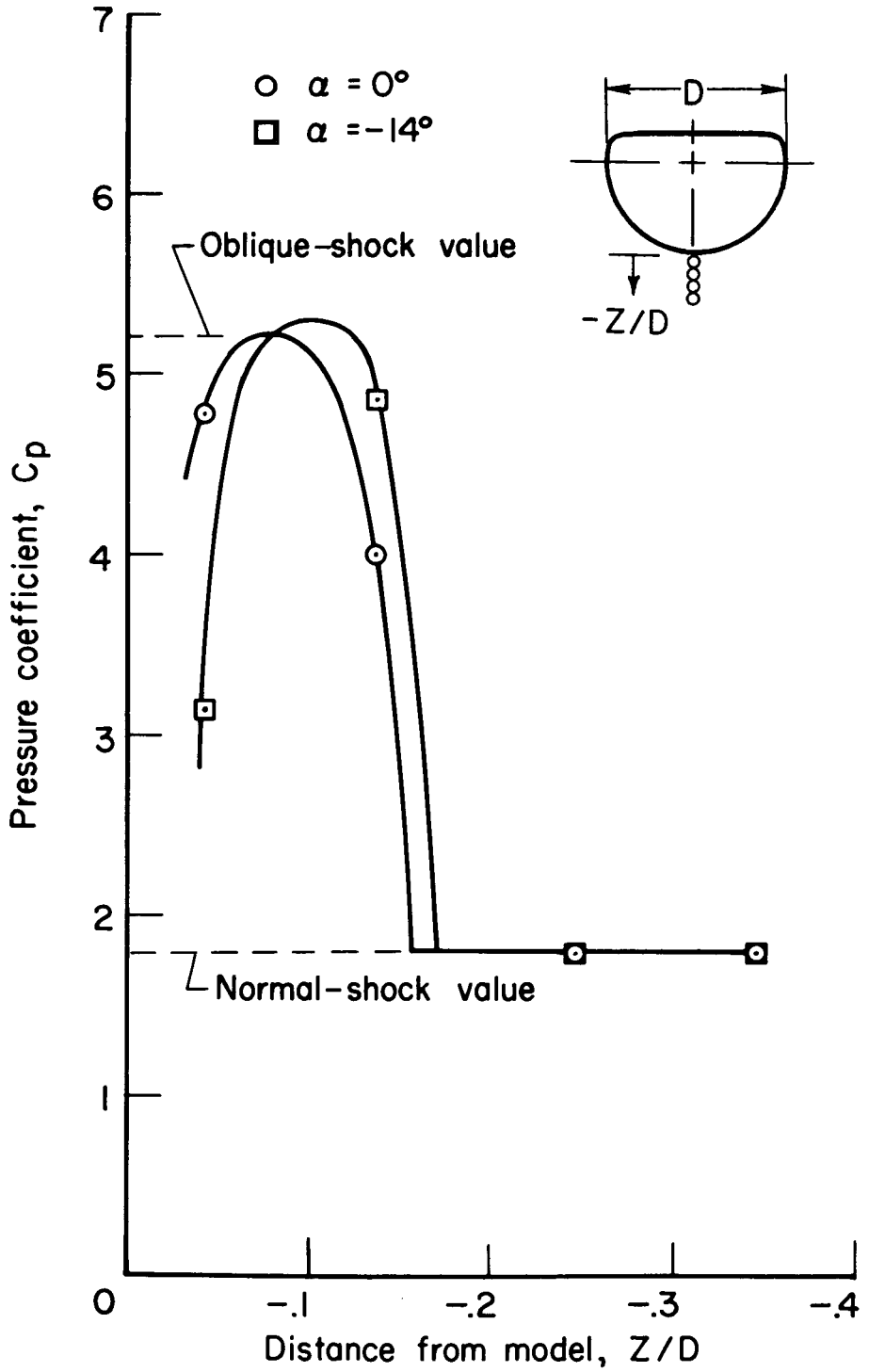

(a) Lower rake.

Figure 9.- Body total-pressure field (wind tunnel).

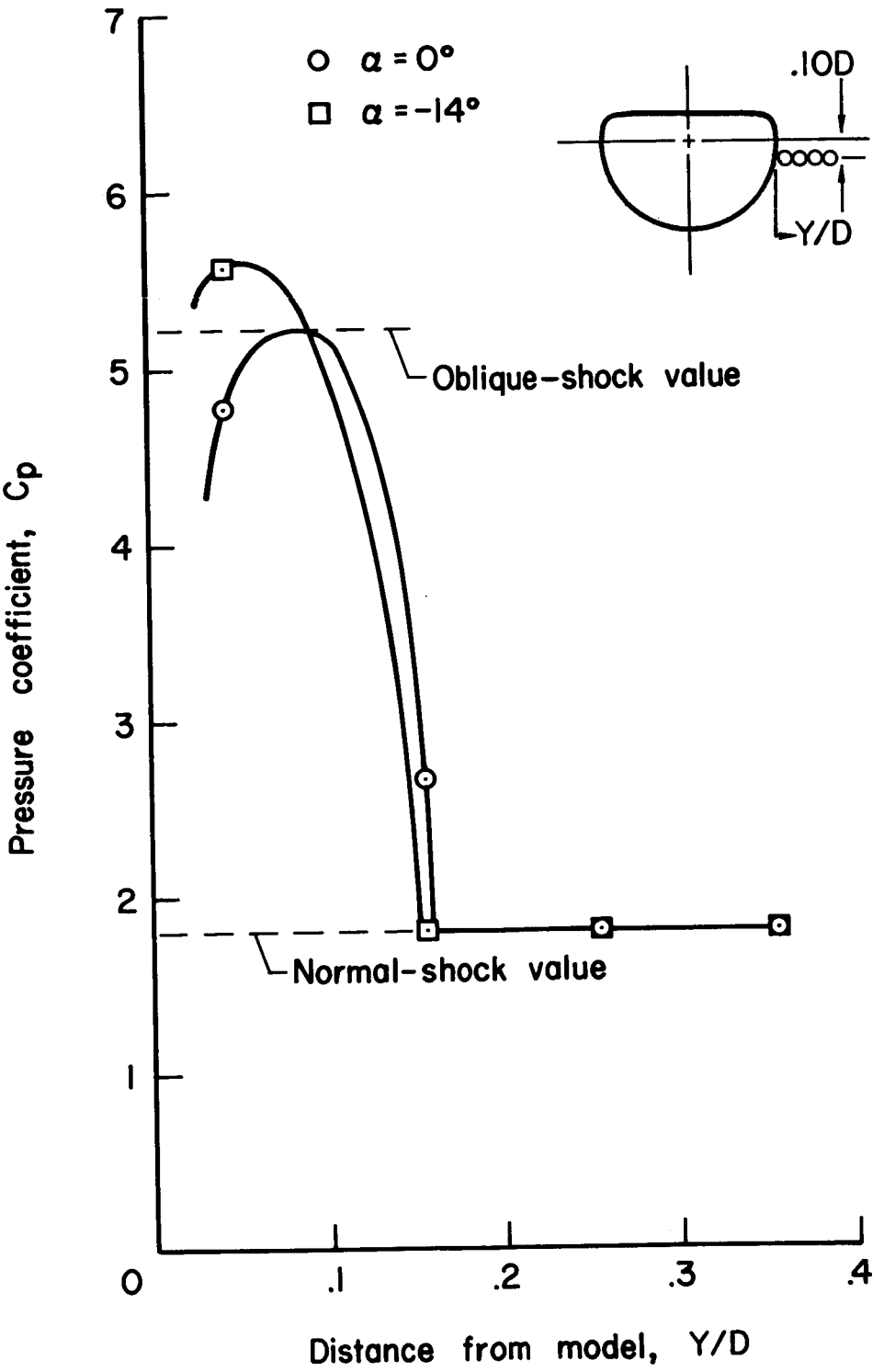

(b) Side rake.

Figure 9.- Continued.

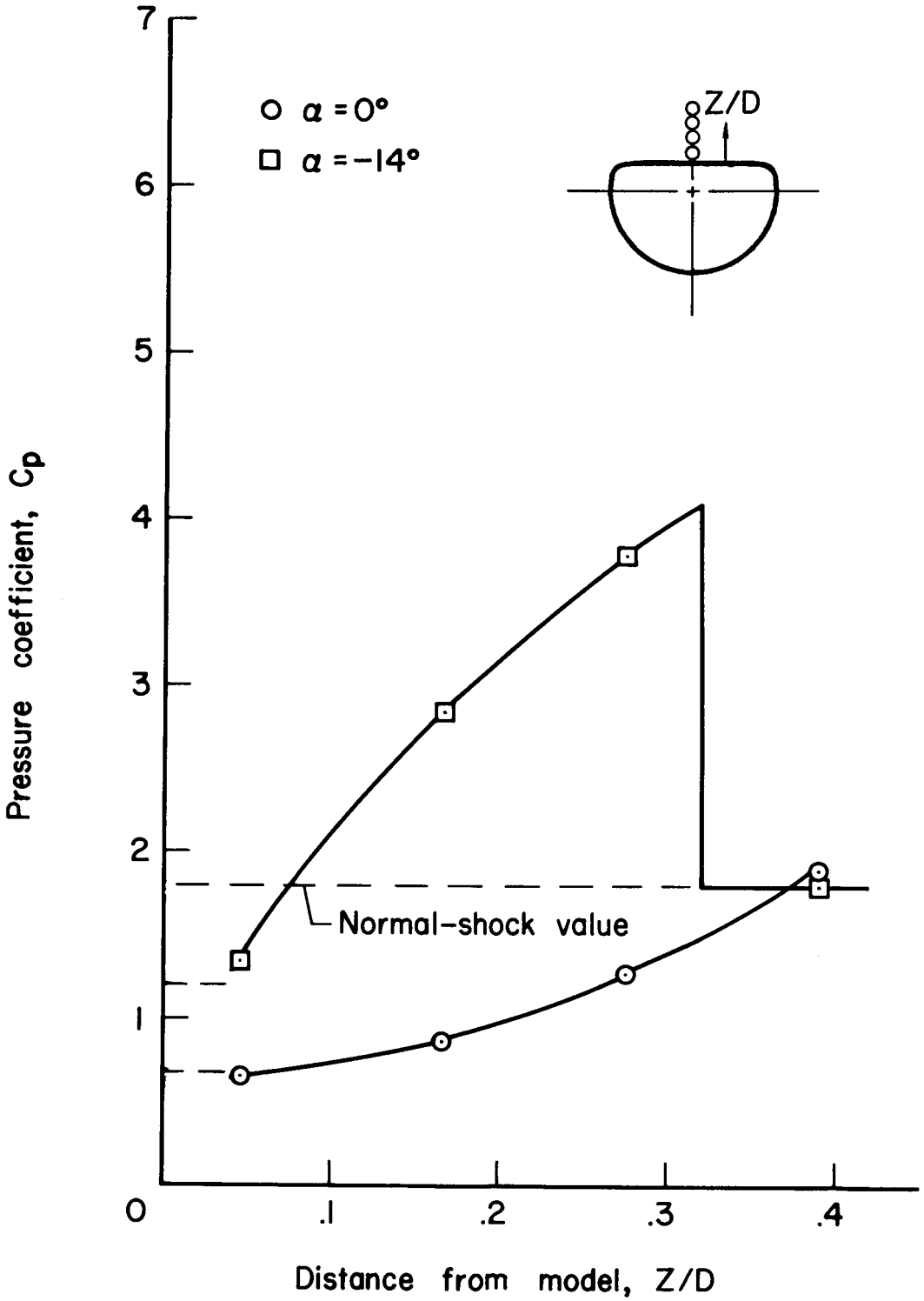

(c) Upper rake.

Figure 9.- Concluded.

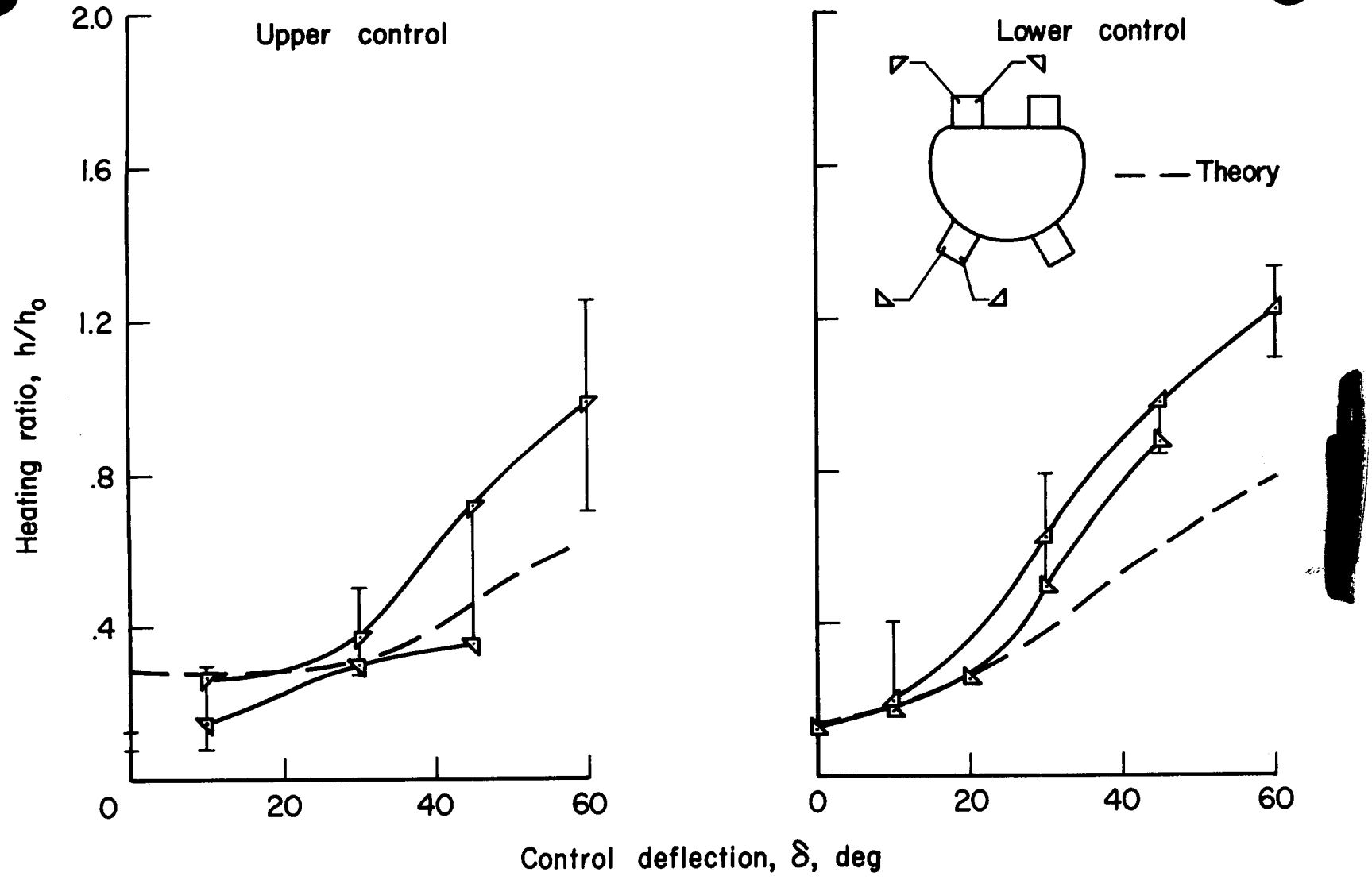

(a) $\alpha = 0^{\circ}$, wind tunnel.

Figure 10.- Variation of control set I heating with deflection angle.

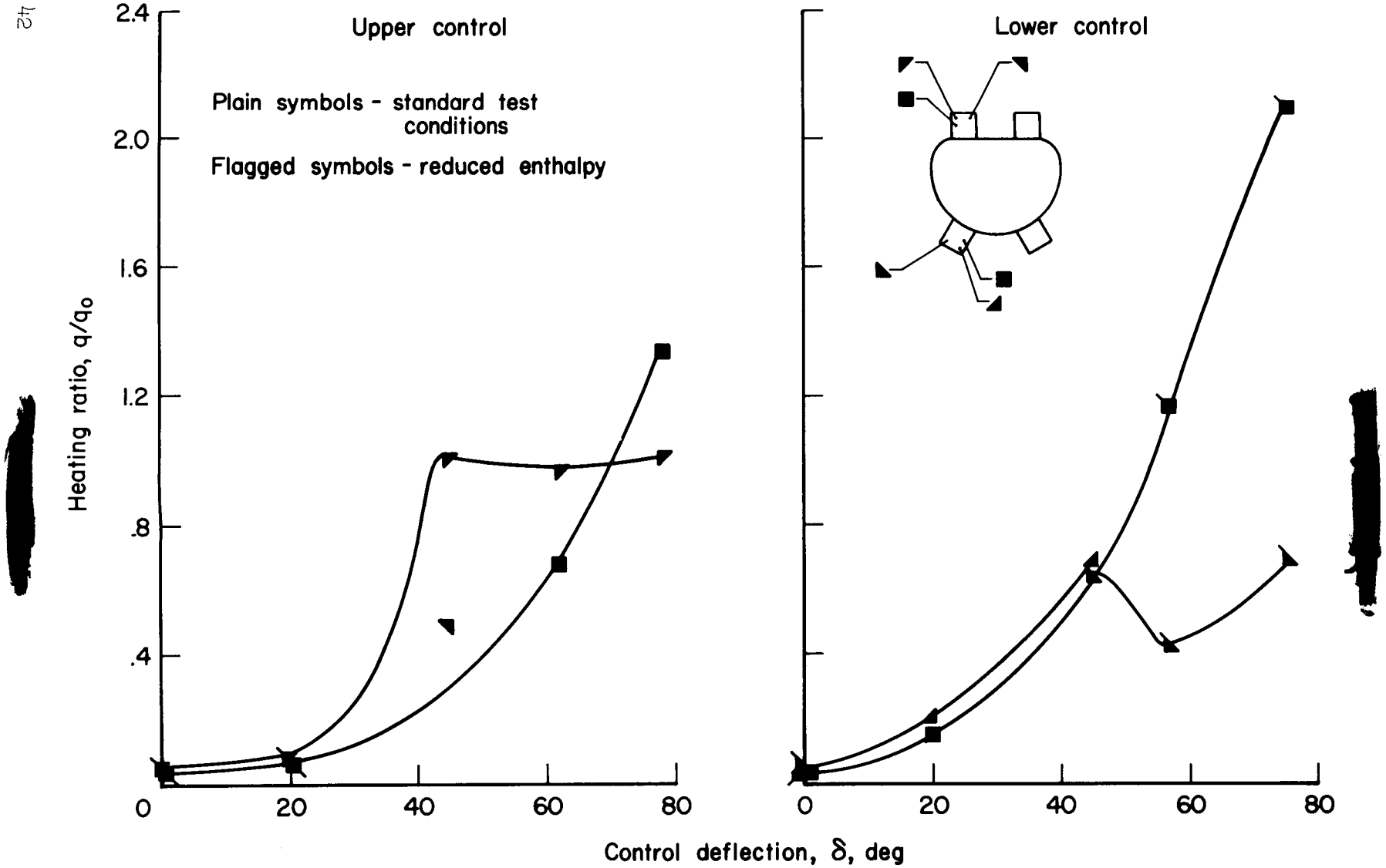

(b) $\alpha = 0^{\circ}$, shock tunnel.

Figure 10.- Continued.

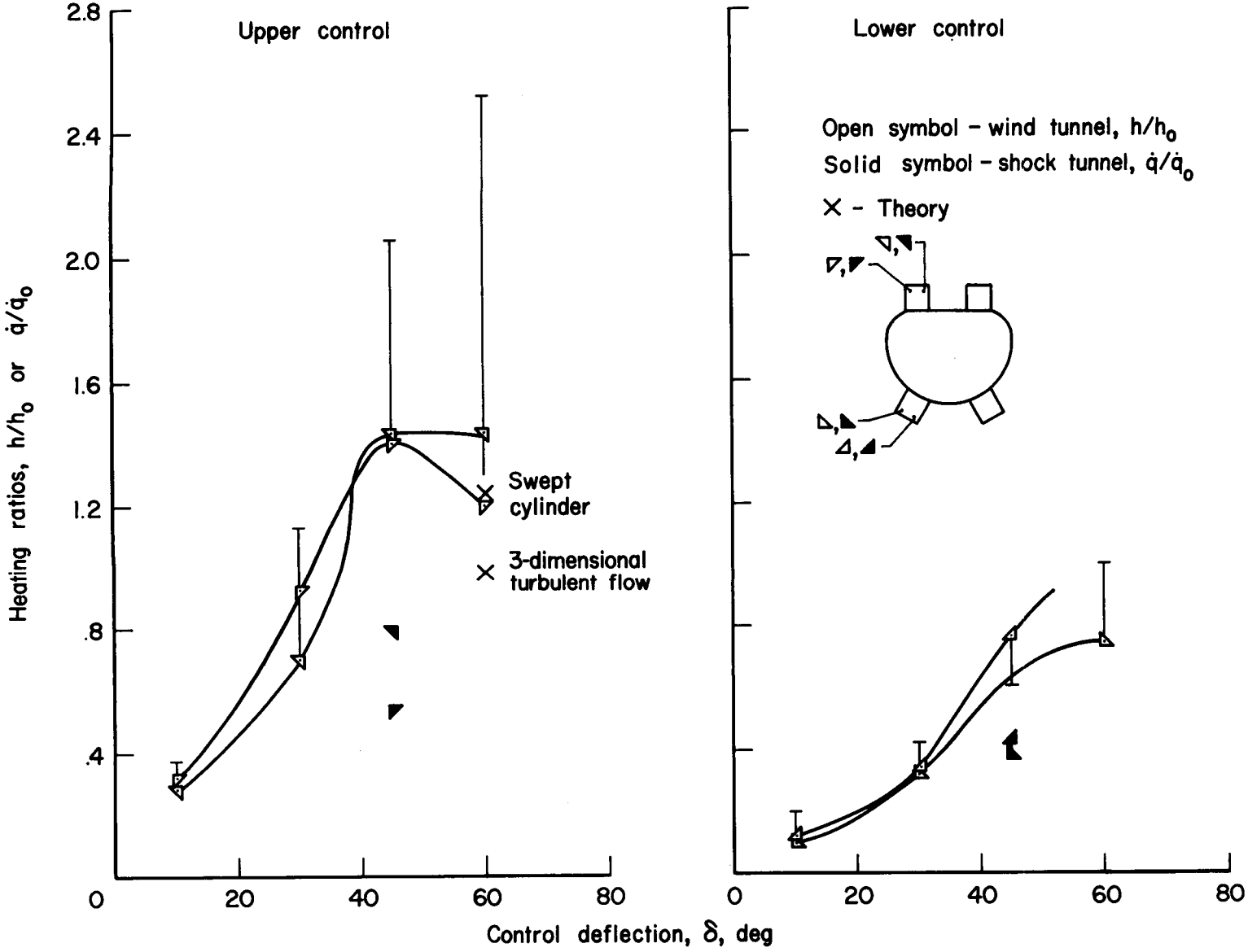

(c) $\alpha = -14^{\circ}$

Figure 10.- Concluded.

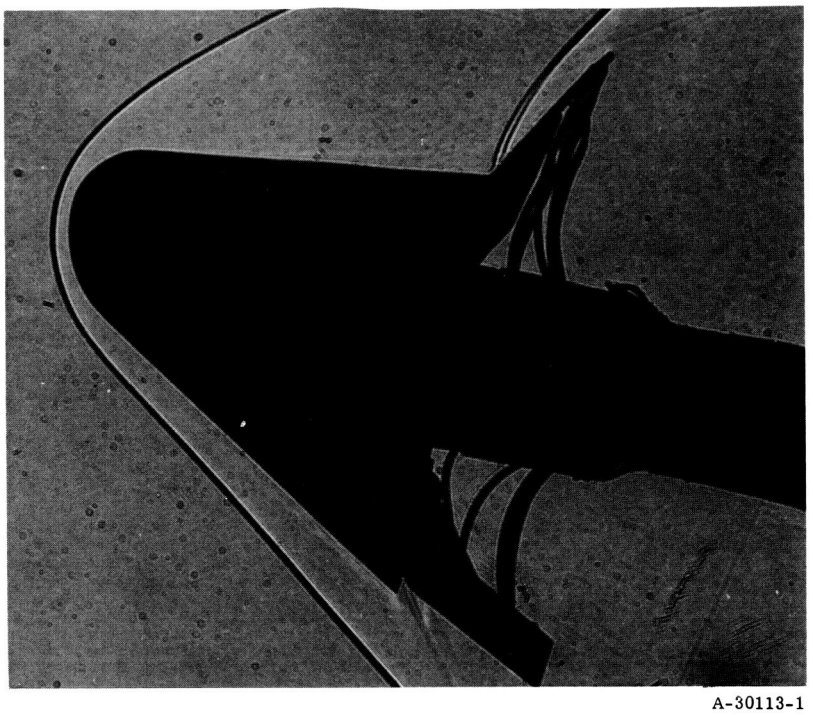

A-30113-1

(a) Upper controls $\delta = 60^{\circ}$; lower controls $\delta = 30^{\circ}$; $\alpha = 4^{\circ}$

A-30113-2

(b) Upper controls $\delta = 45^{\circ}$ and 60°; lower controls $\delta = 10^{\circ}$ and 30°; $\alpha = -14^{\circ}$.

Figure 11.- Shadowgraphs of flow about the wind-tunnel model with control set

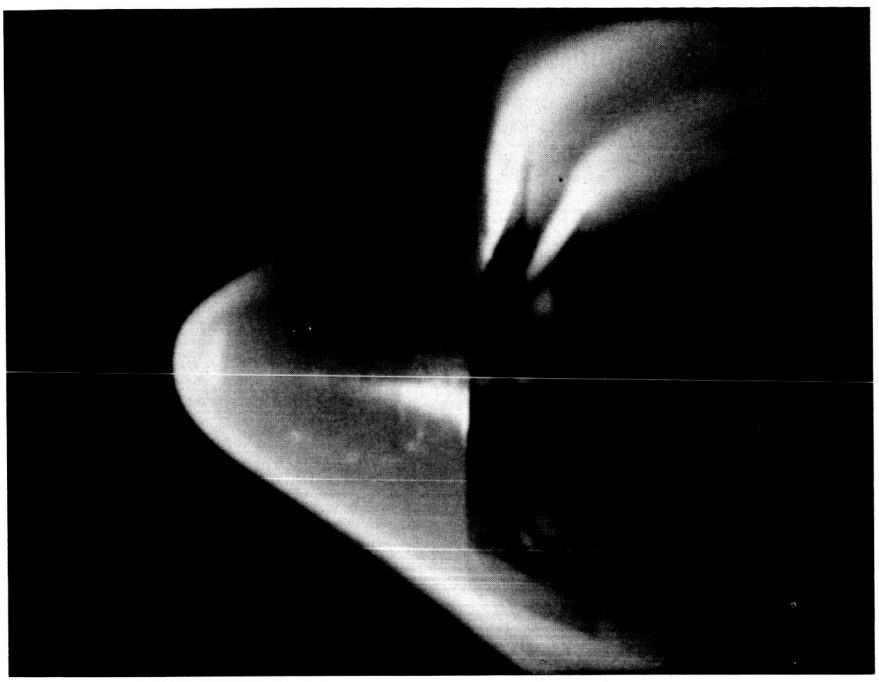

A-30113-3

(a) Self-luminous photograph of flow; upper controls $\delta = 78^{\circ}$ and 63°; lower controls $\delta = 0^{\circ}$ and 21°; $\alpha = -0.75^{\circ}$.

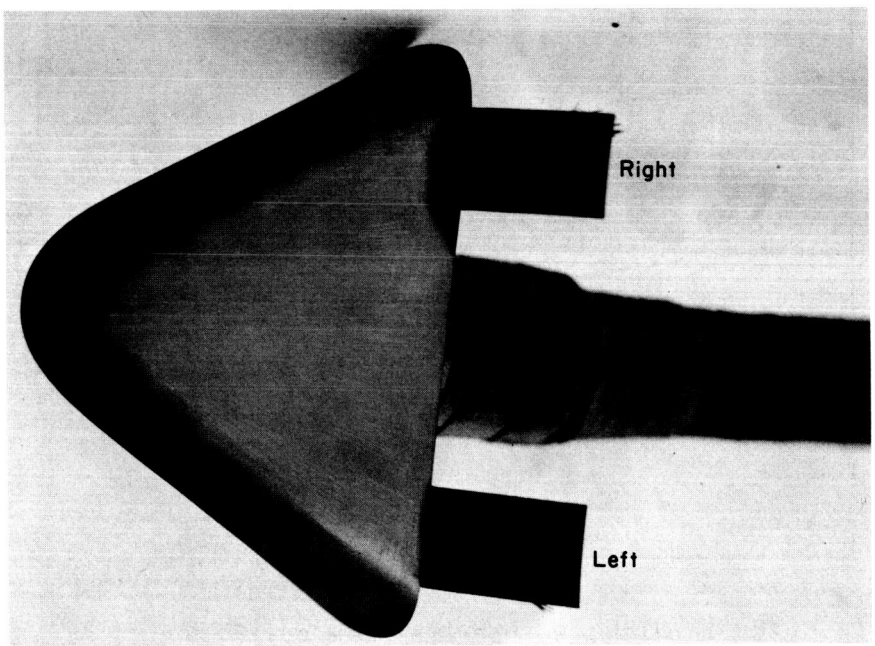

A-30113-4

(b) Model condition after test.

Figure 12.- Photographs of shock-tunnel test model with control set I.

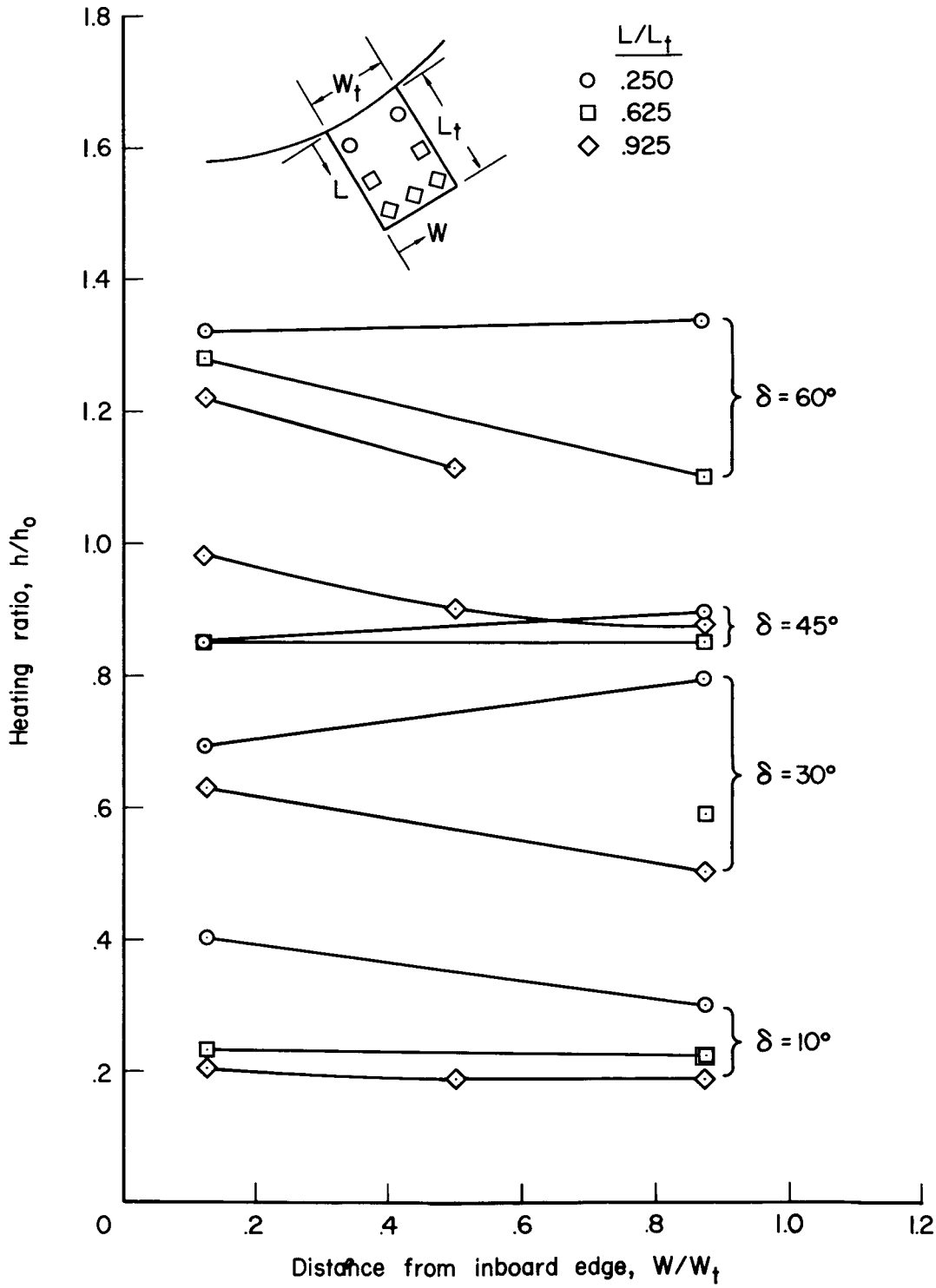

(a) Lower control.

Figure 13.- Spanwise heating distributions for several deflection angles of control set I measured in the wind tunnel at $\alpha = 0^{\circ}$.

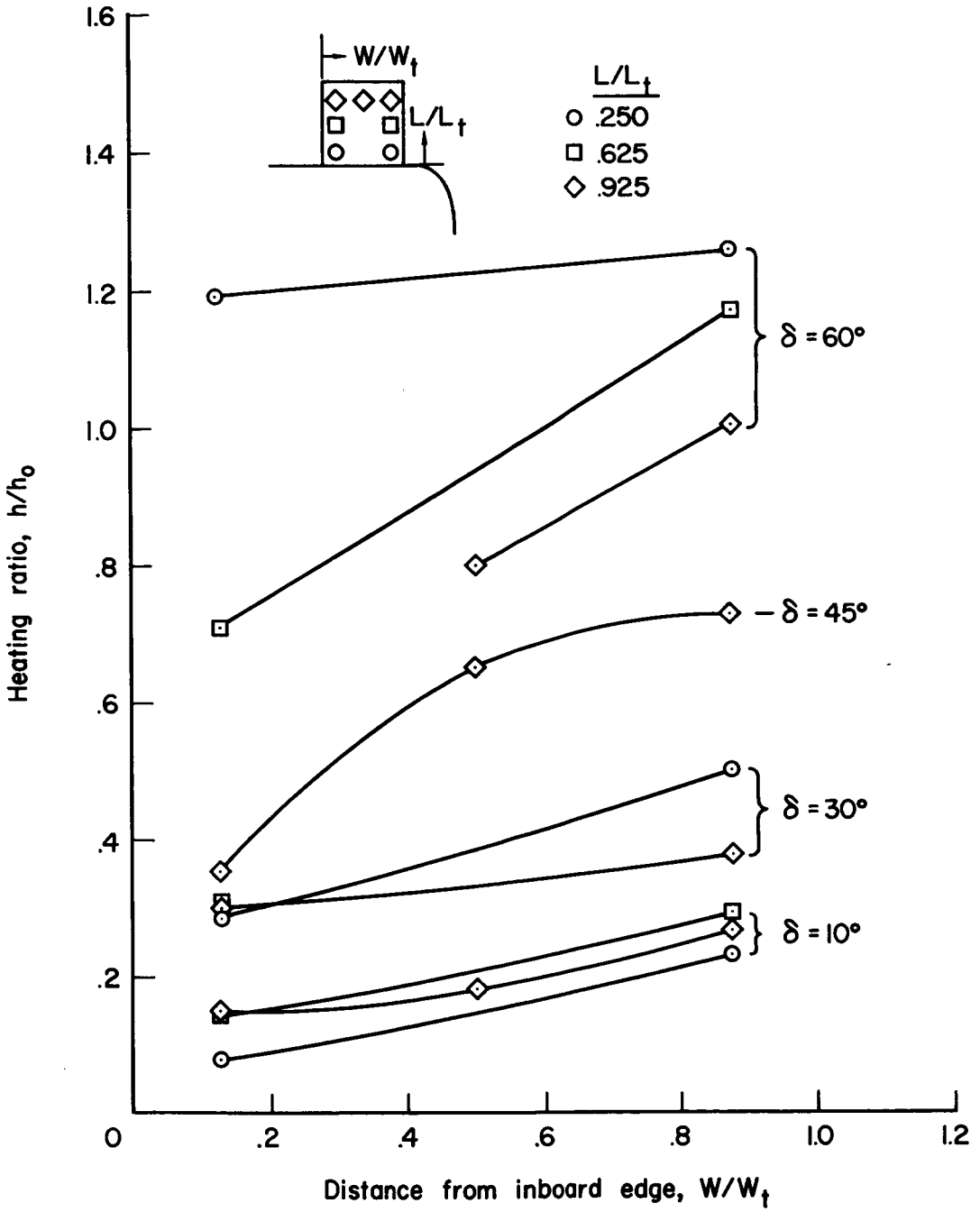

(b) Upper control.

Figure 13.- Concluded.

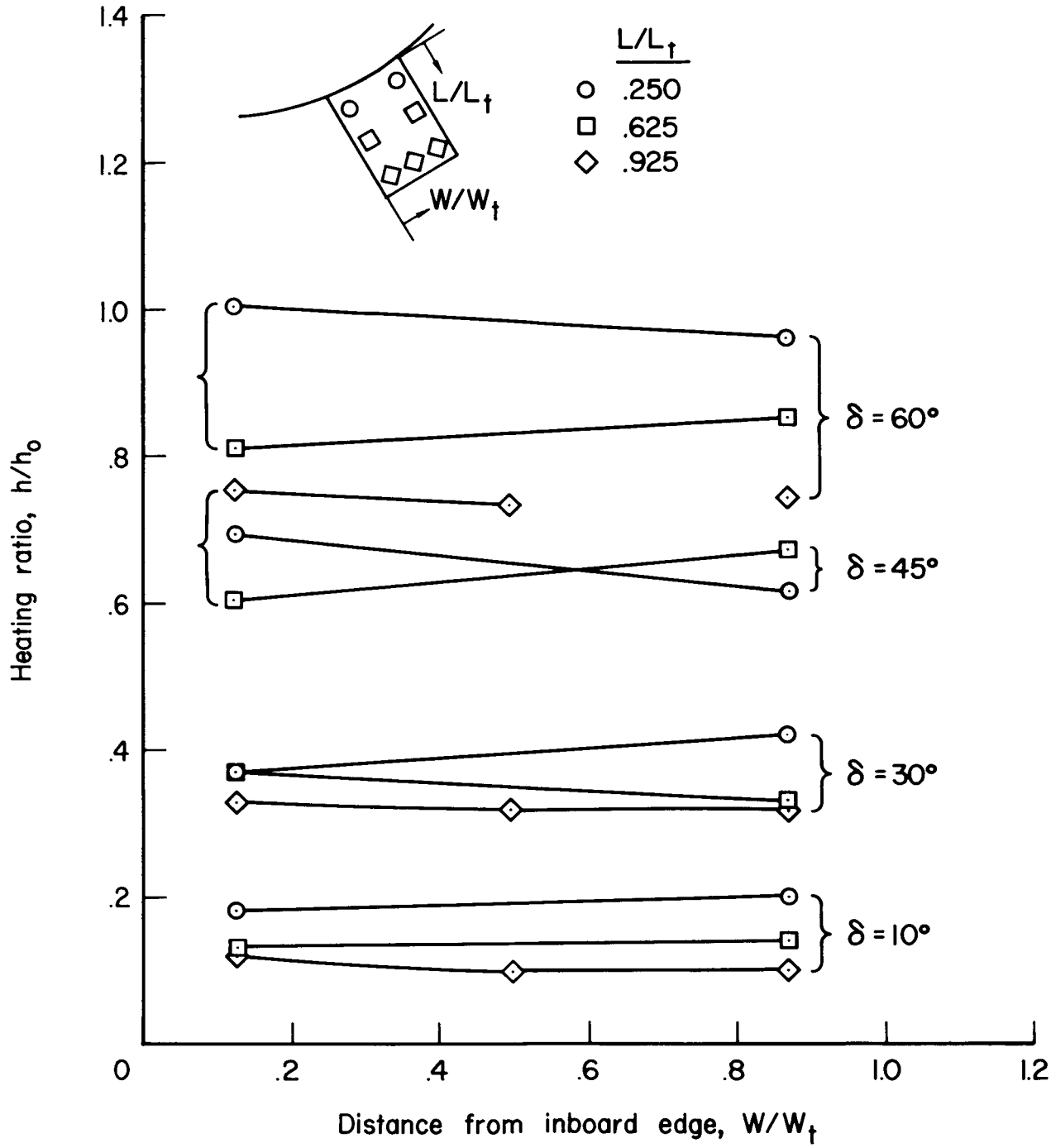

(a) Lower control.

Figure 14.- Spanwise heating distributions for several deflection angles of control set I measured in the wind tunnel at $\alpha = -14^{\circ}$.

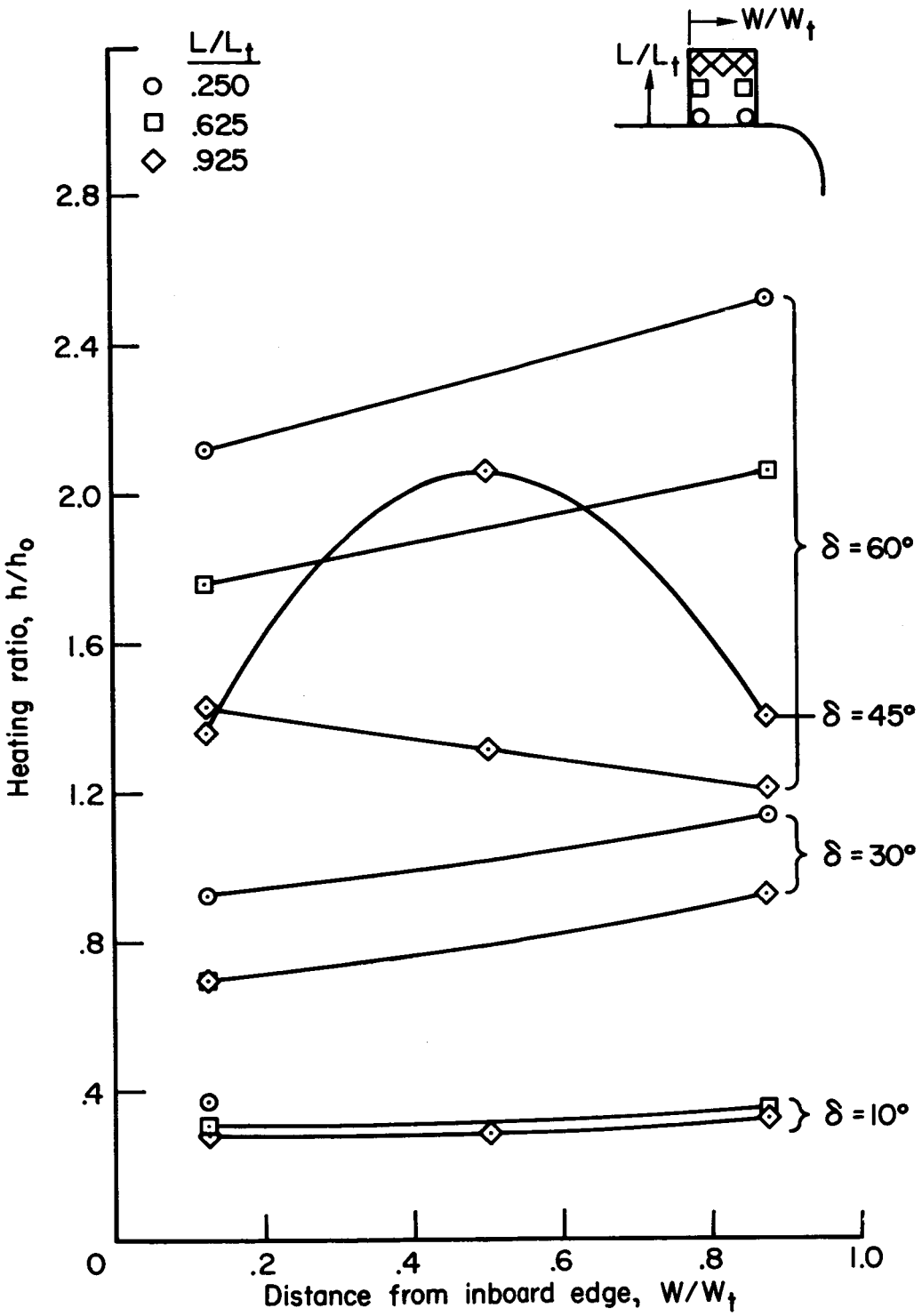

(b) Upper control.

Figure 14.- Concluded.

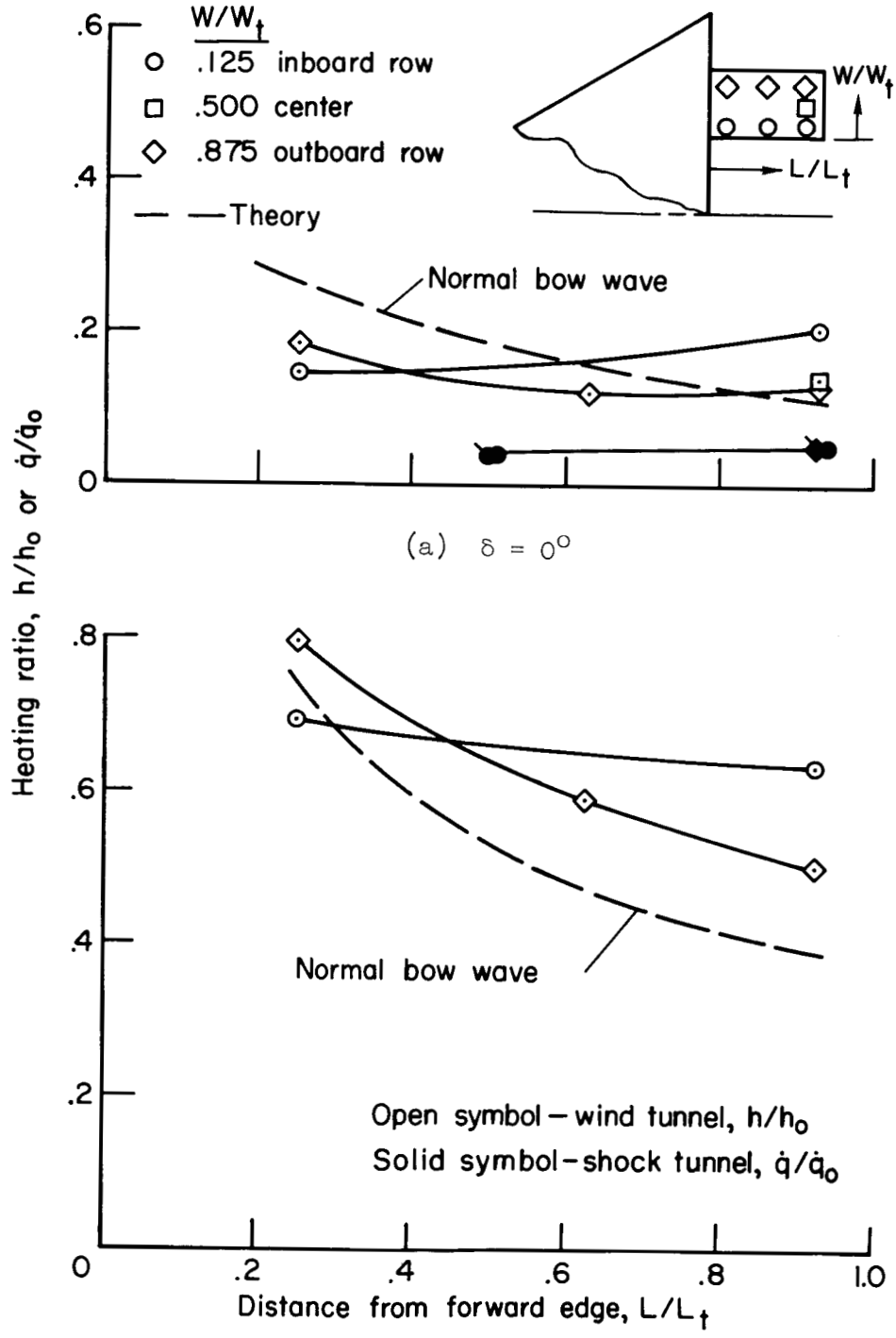

Figure 15.- Longitudinal heating distributions for several deflection angles of the lower flap of control set I measured at $\alpha = 0^{\circ}$.

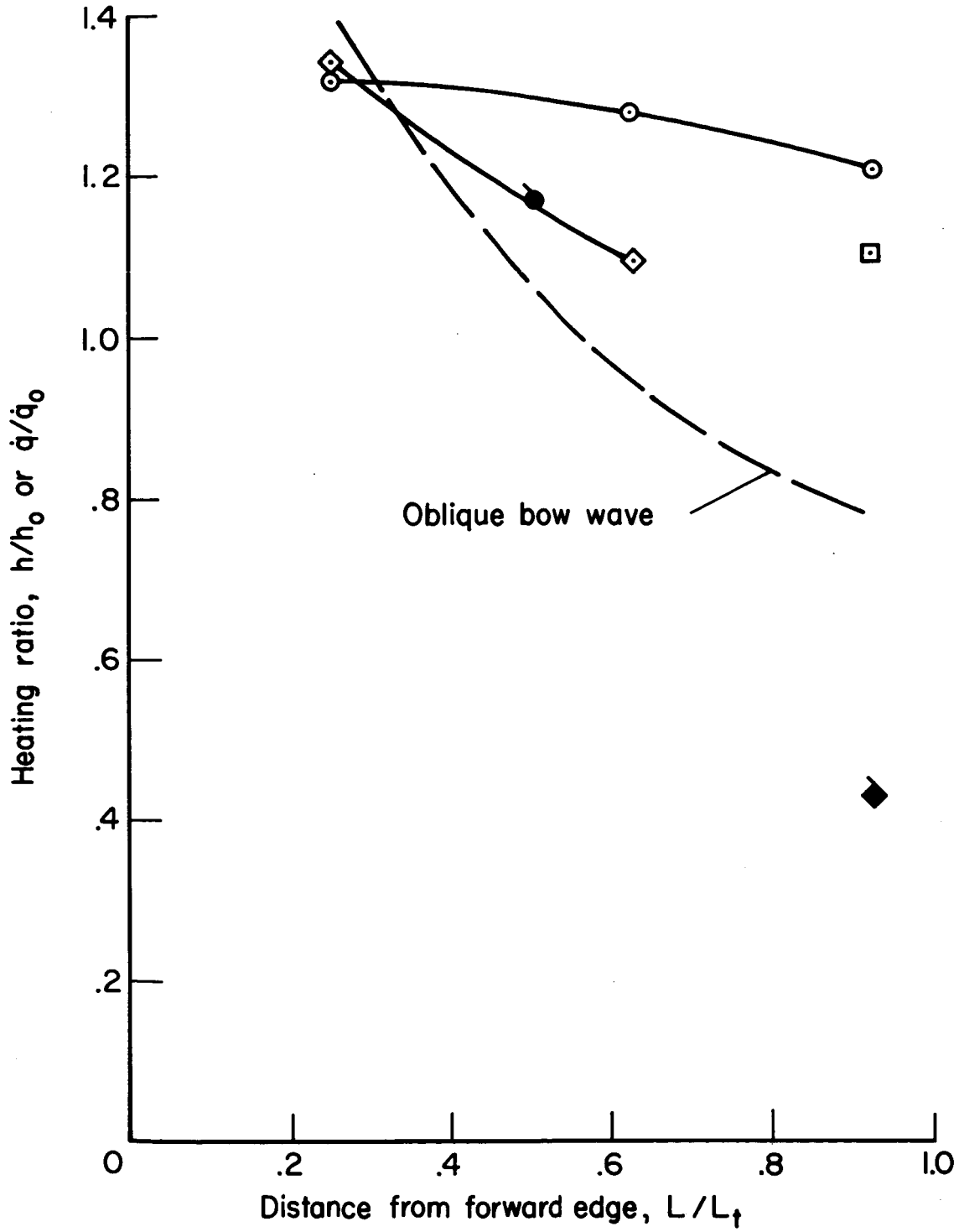

(c) $\delta = 60^\circ$

Figure 15.- Concluded.

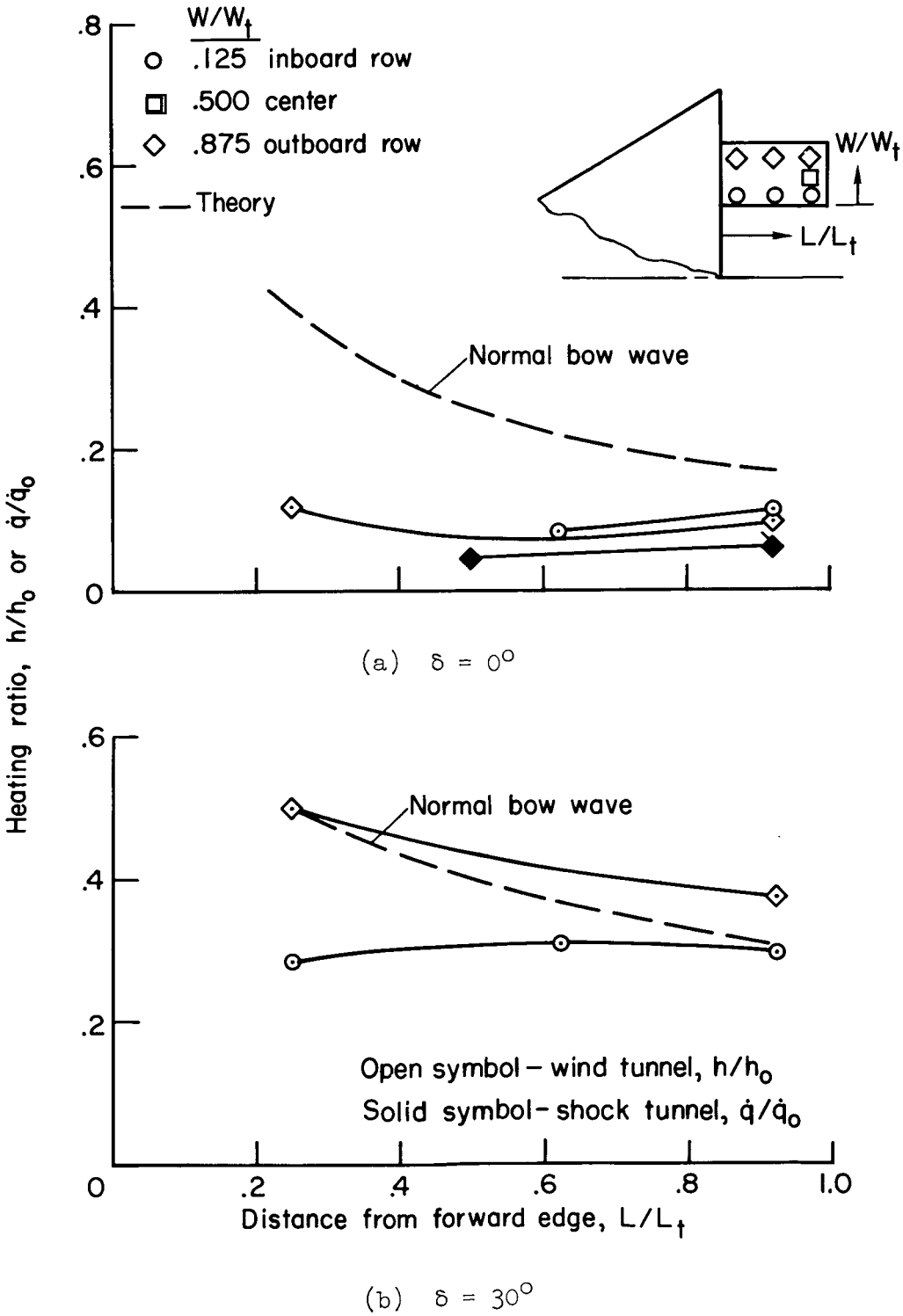

Figure 16.- Longitudinal heating distributions for several deflection angles of the upper flap of control set I measured at $\alpha = 0^{\circ}$.

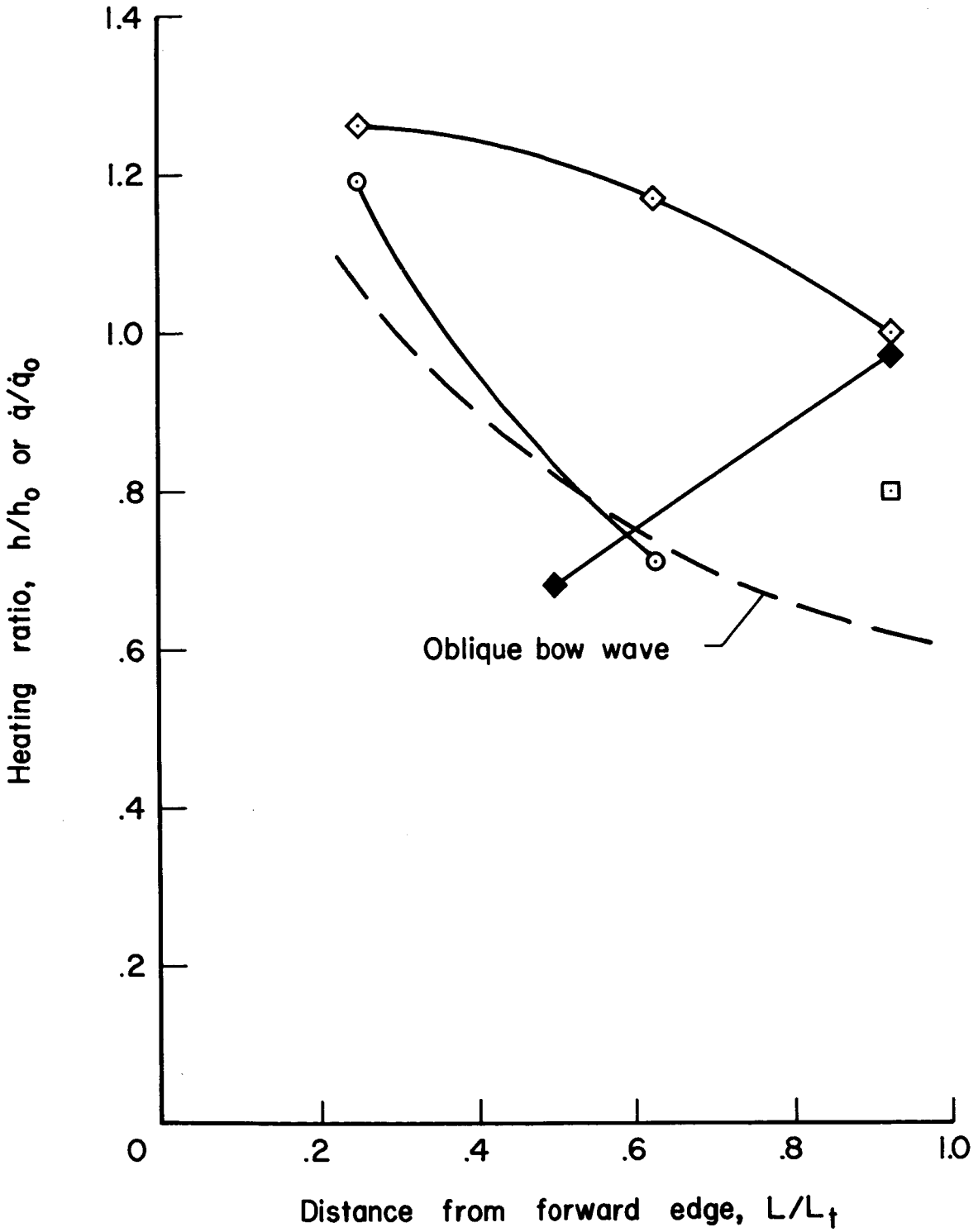

(c) $\delta = 60^\circ$

Figure 16.- Concluded.

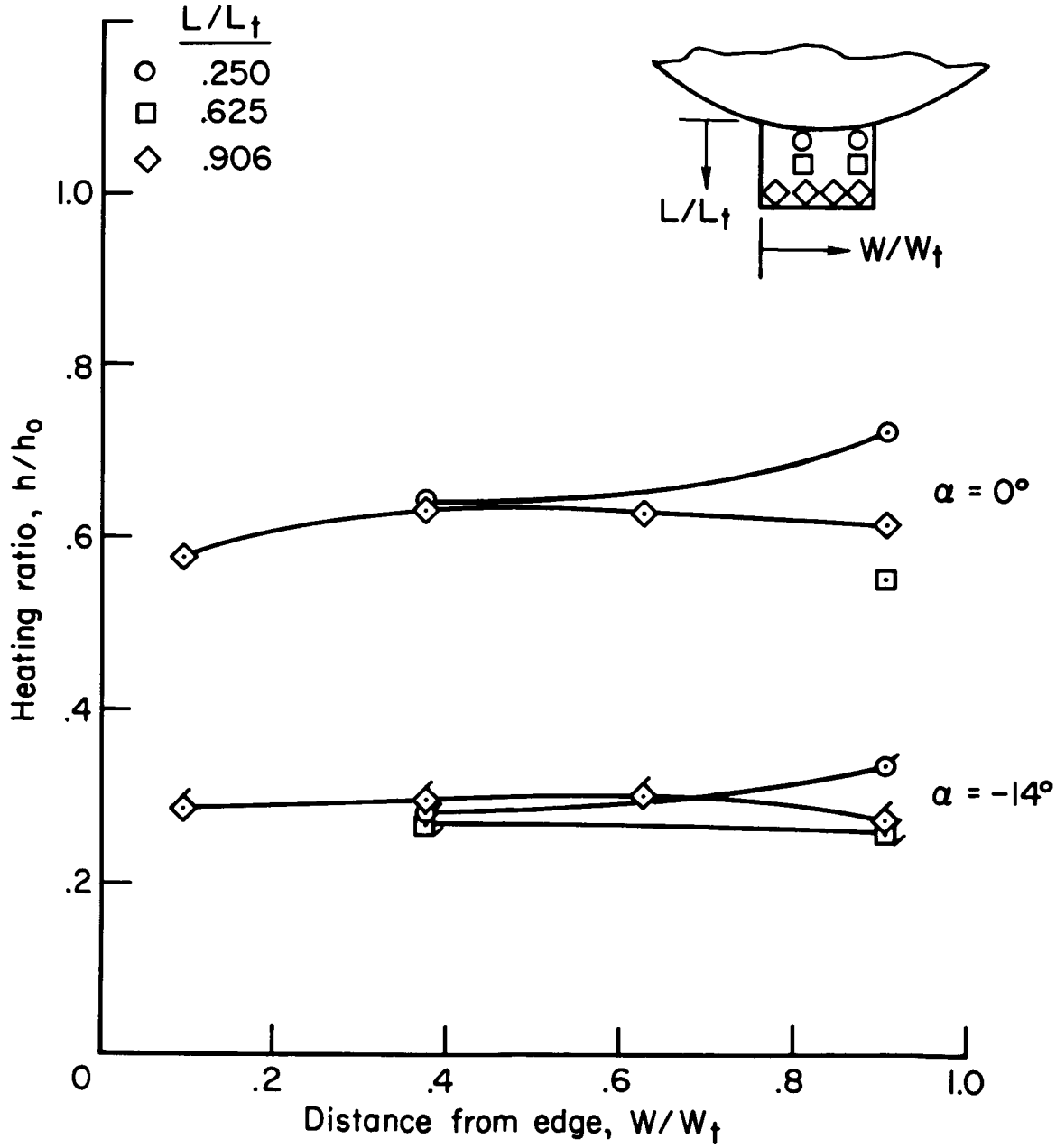

(a) Lower control

Figure 17.- Spanwise heating distributions for control set II at a deflection angle of 25° measured in the wind tunnel at $\alpha = 0^{\circ}$ and -14°.

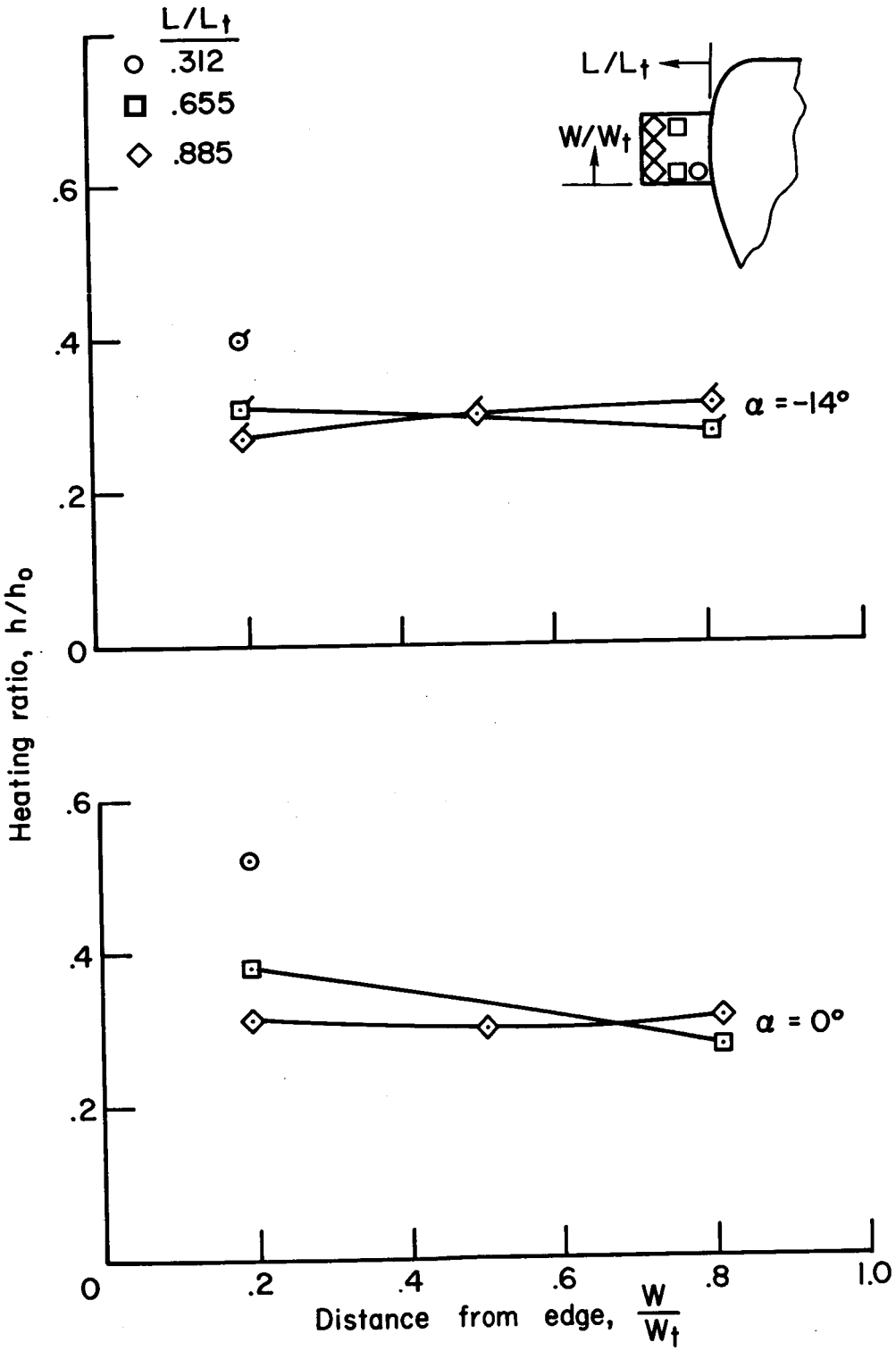

(b) Yaw control.

Figure 17.- Continued.

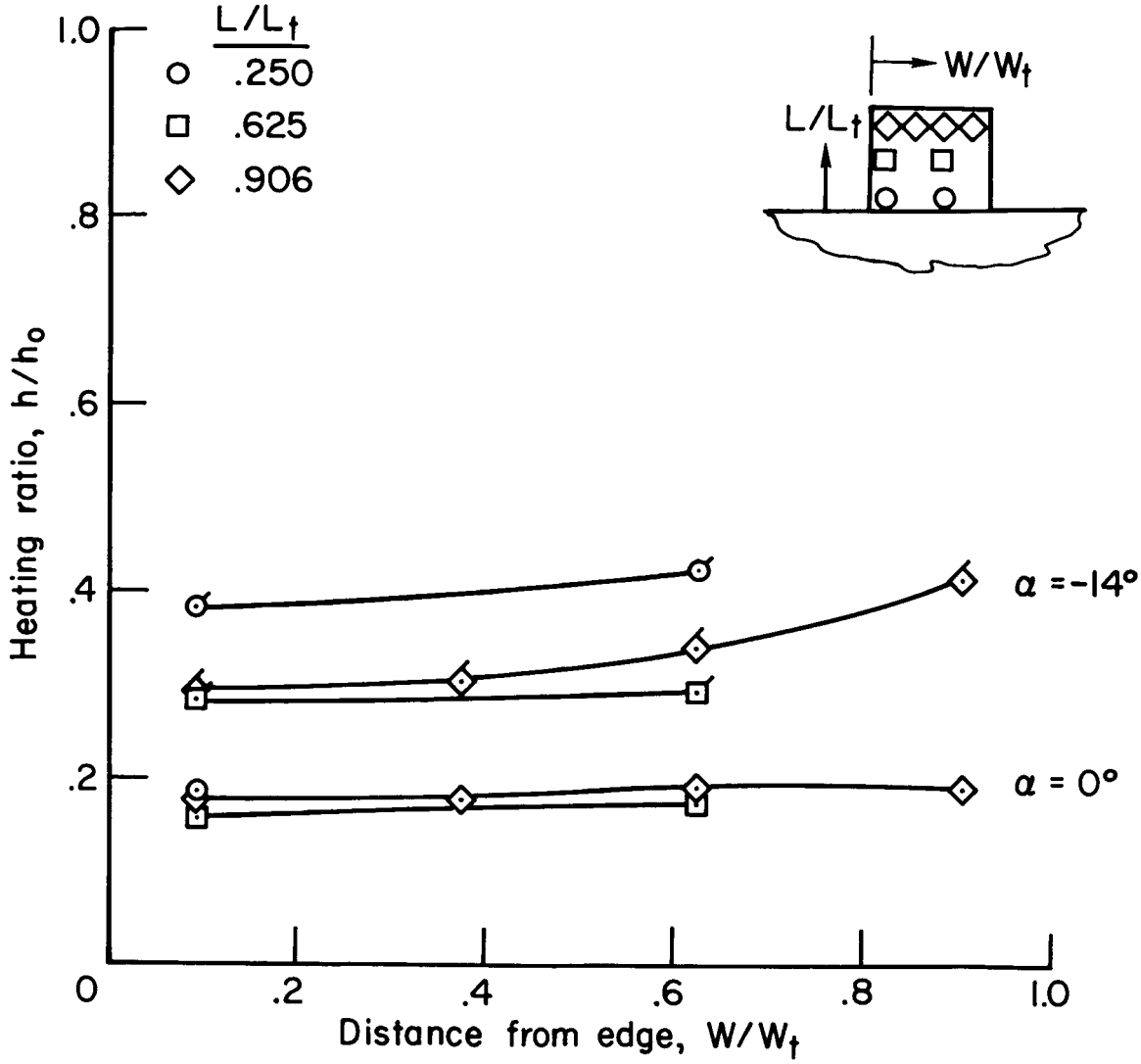

(c) Upper control.

Figure 17.- Concluded.

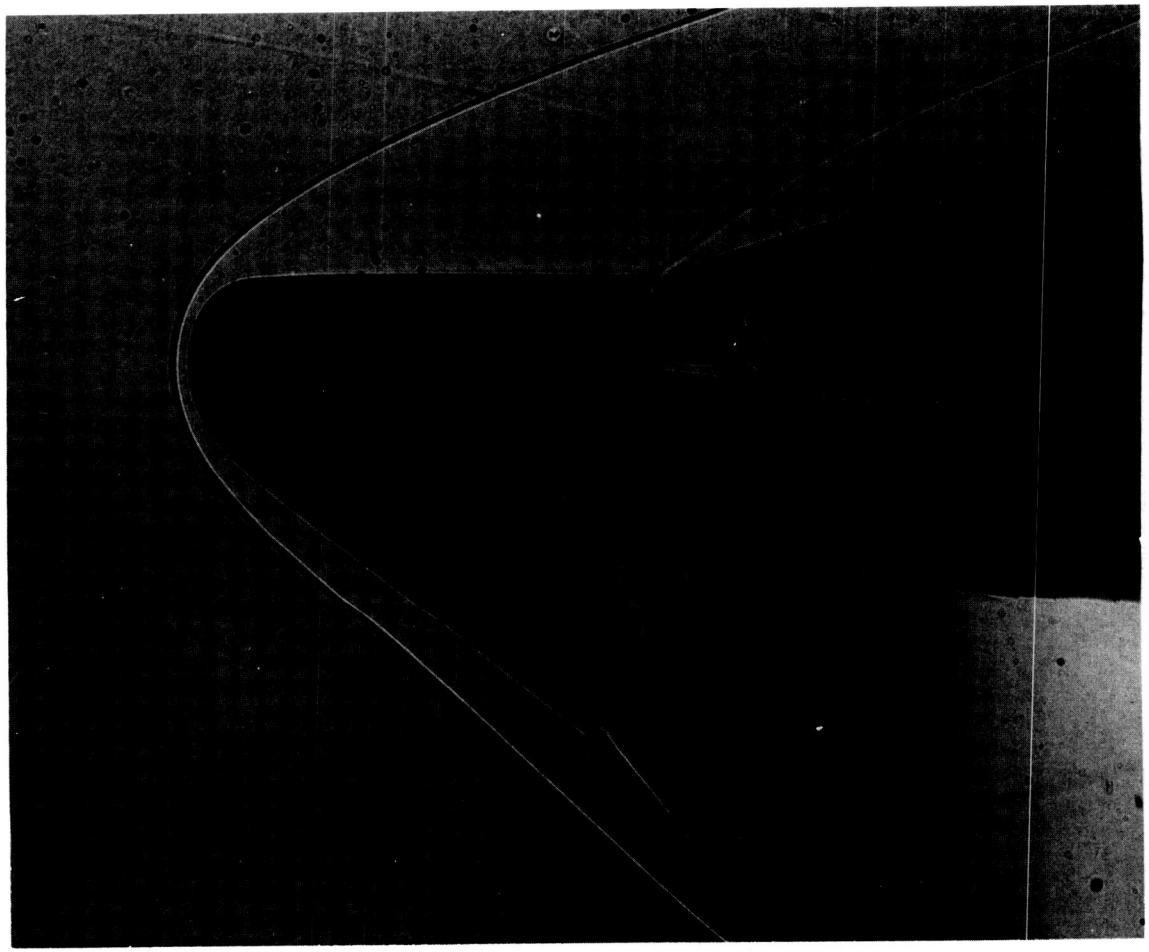

A-30113-5

Figure 18.- Shadowgraph of the flow about the wind-tunnel model with control set II; upper controls $\delta = 25^{\circ}$; lower controls $\delta = 25^{\circ}$; $\alpha = 0^{\circ}$.

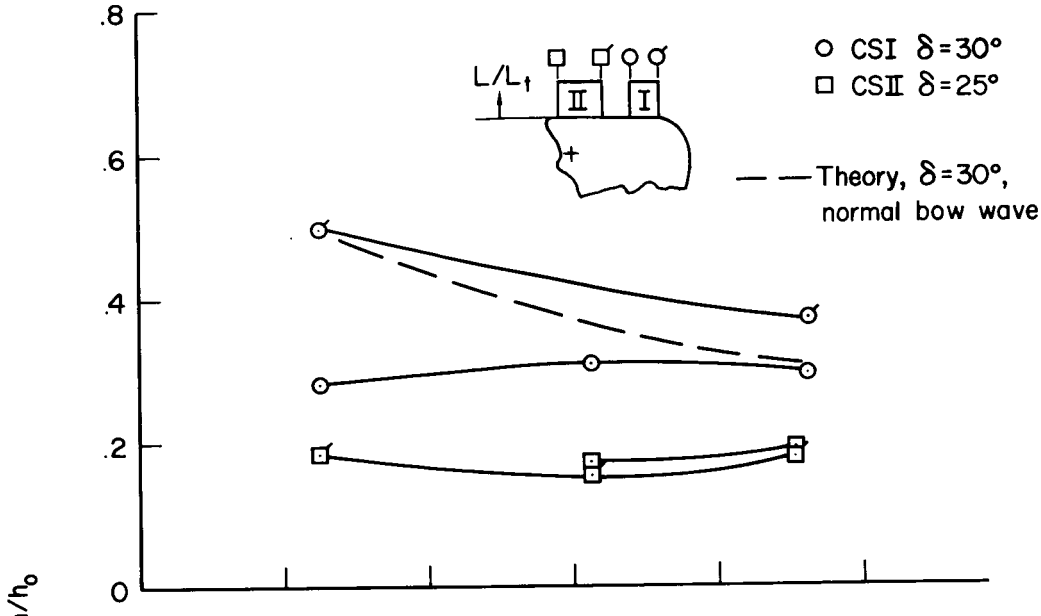

(a) Upper controls.

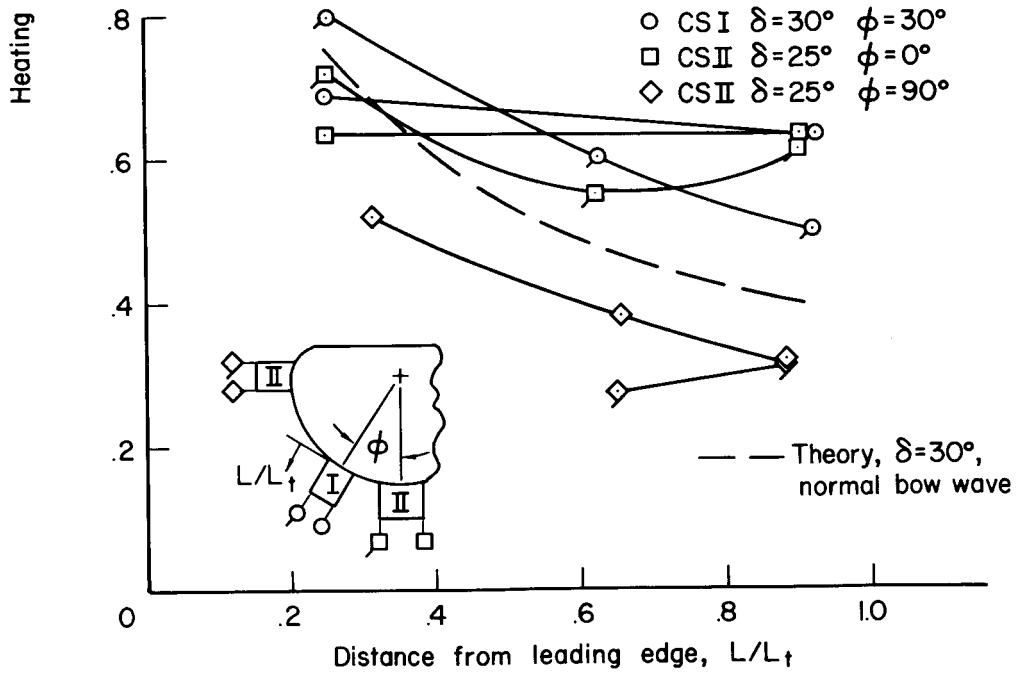

(b) Lower and yaw controls.

Figure 19.- Heating ratios for control sets I and II measured in the wind tunnel at $\alpha = 0^{\circ}$.

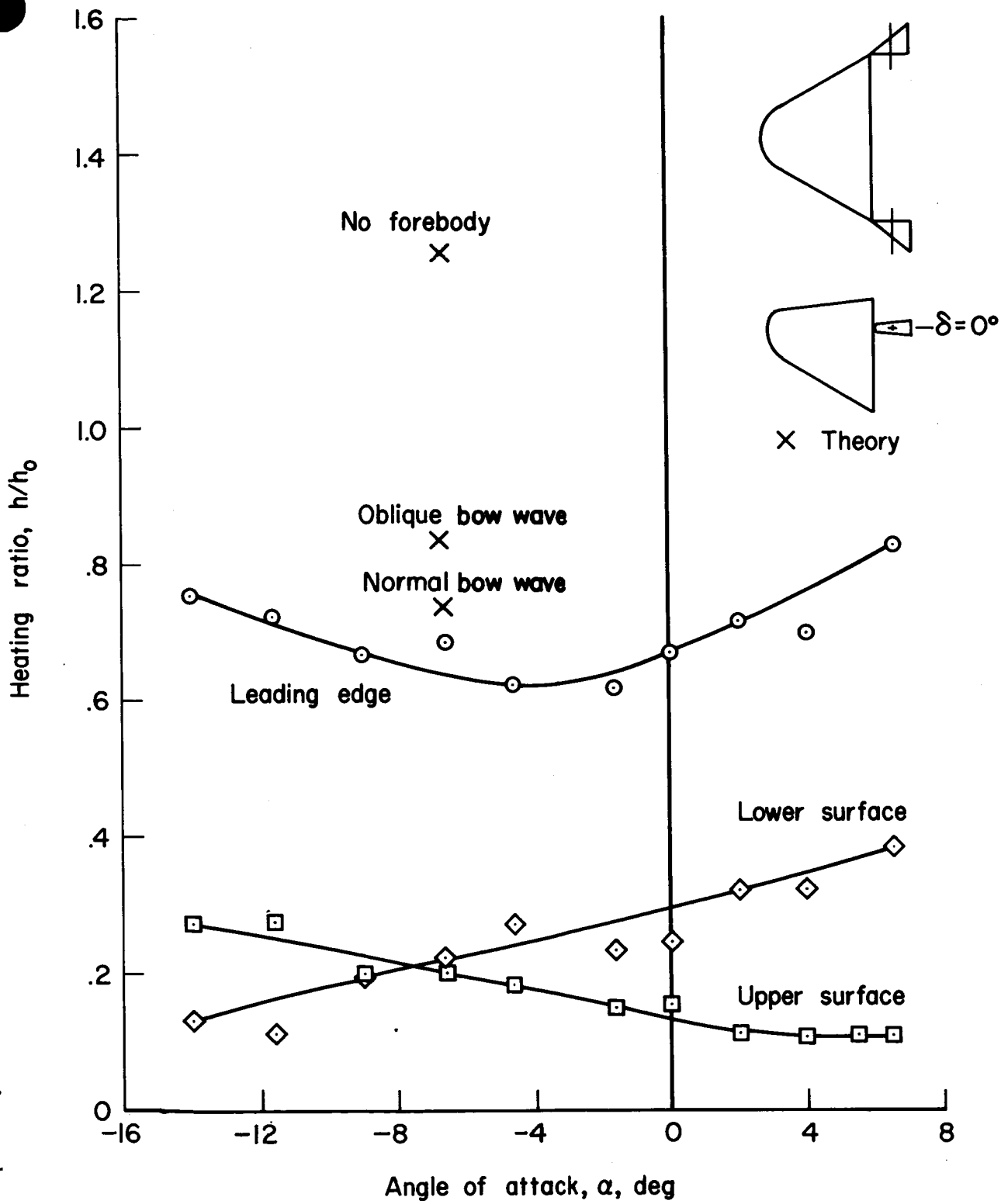

Figure 20.- Variation of heating ratios with angle of attack for the undeflected elevon (wind tunnel).

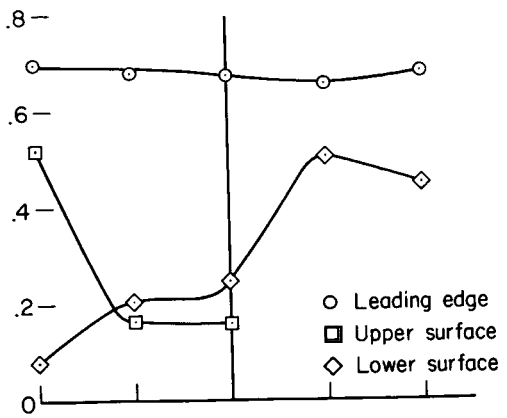

(a) $\alpha = 0^{\circ}$

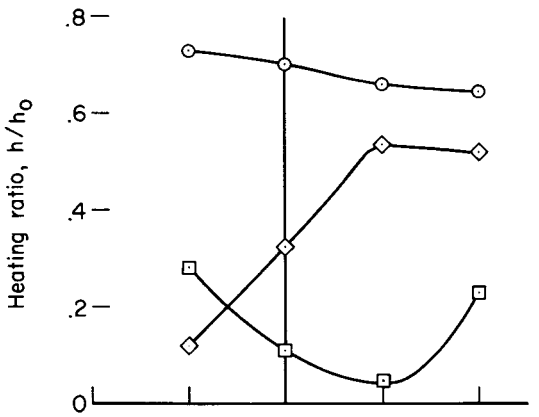

(b) $\alpha = 4^{\circ}$

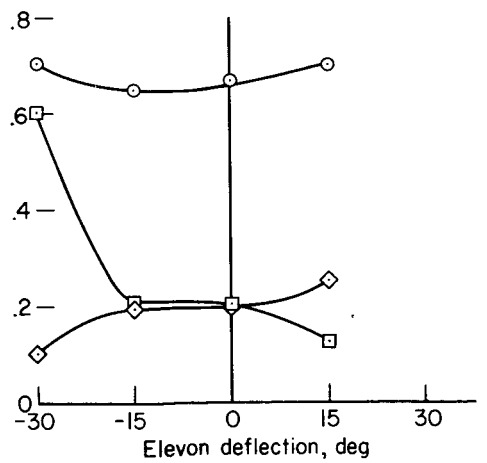

(c) $\alpha = -9^{\circ}$

Figure 21.- Variation of elevon heating ratios with deflection angle (wind tunnel).

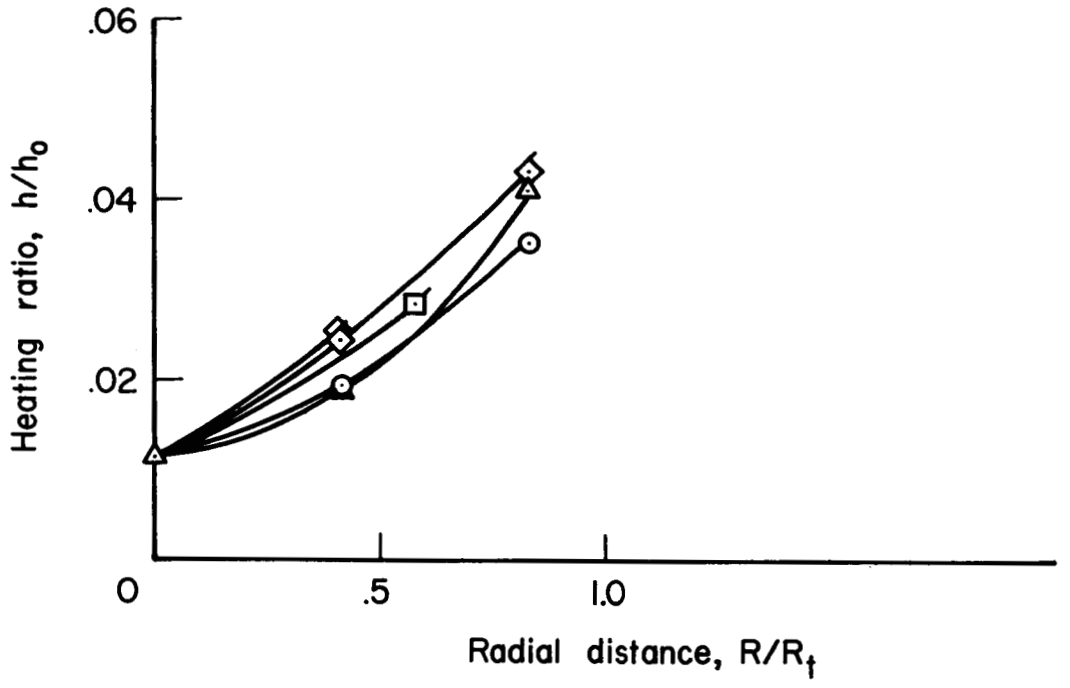

(a) $\alpha = 4^o$, lower controls off (top support).

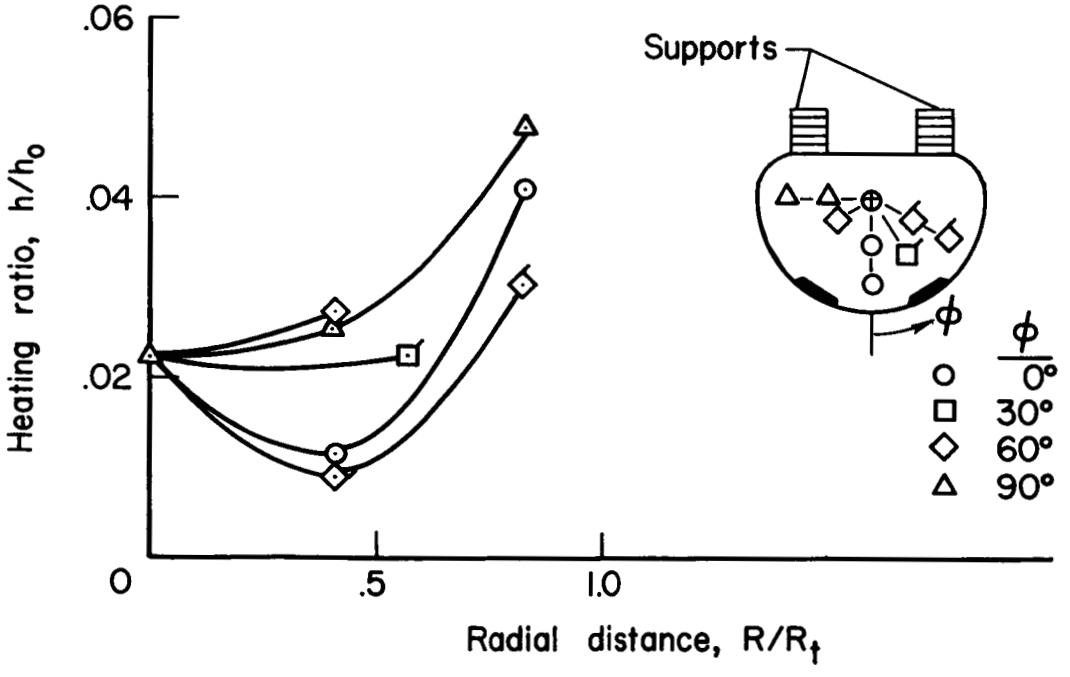

(b) $\alpha = 1^o$, $\delta = 0^o$ (top support).

Figure 22.- Base heating distributions for various angles of attack and deflection angles of control set I (wind tunnel).

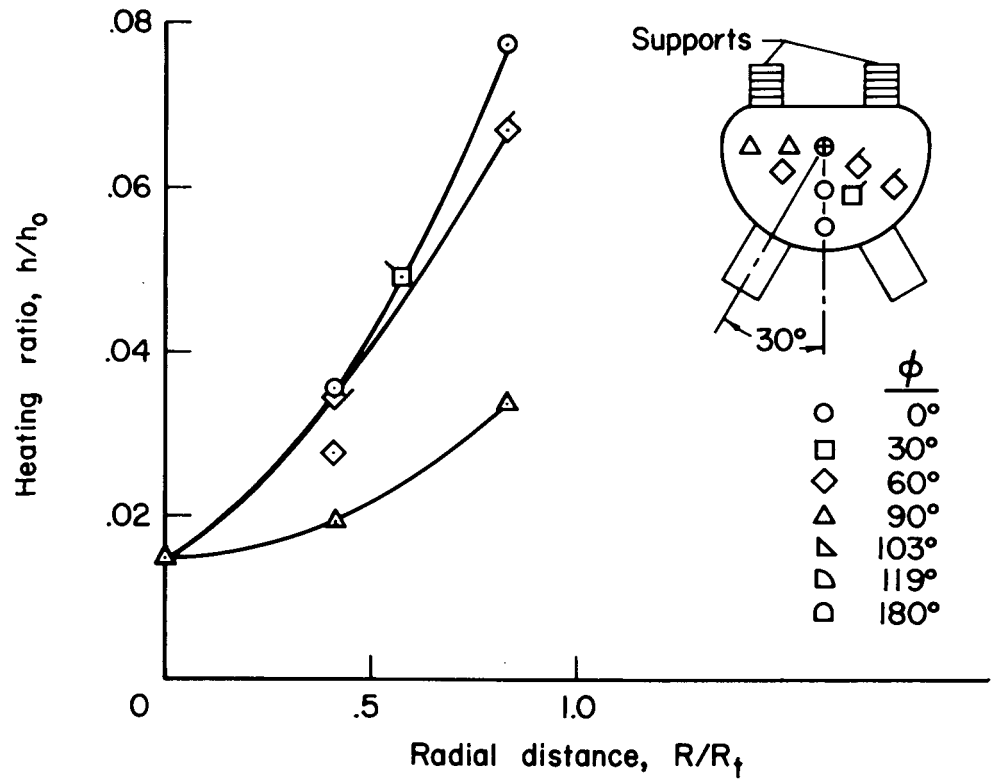

(c) $\alpha = 4^{\circ}$, $\delta = 60^{\circ}$ (top support).

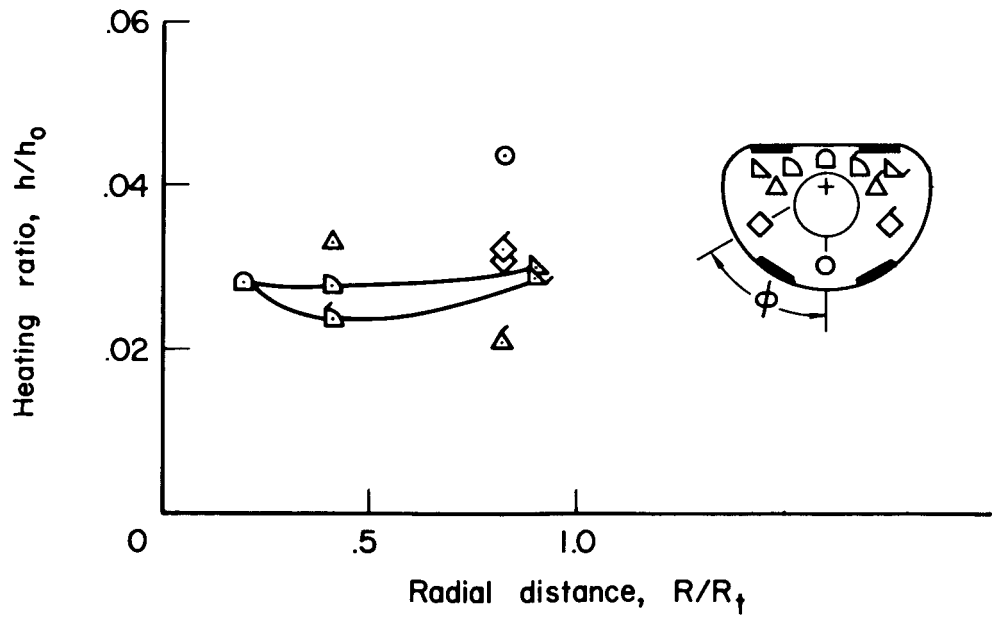

(d) $\alpha = 0^{\circ}$, $\delta = 0^{\circ}$ (sting support).

Figure 22.- Concluded.

NASA-Langley, 1963 A-490